NASA Technical Memorandum 80178

Single Pilot Scanning Behavior In Simulated Instrument Flight

Jack E. Pennington

October 1979

(NASA-TM-80178) SINGLE PILOT SCANNING BEHAVIOR IN SIMULATED INSTRUMENT FLIGHT (NASA) 55 p HC A04/MF A01 CSCL 05I

N80-12732

Unclas
G3/53 46160

NASA
National Aeronautics and Space Administration

Langley Research Center
Hampton, Virginia 23665

SINGLE PILOT SCANNING BEHAVIOR IN SIMULATED INSTRUMENT FLIGHT

Jack E. Pennington

INTRODUCTION

General Aviation (GA) includes the largest number of aircraft, pilots, operations, miles flown, accidents, and fatalities in the air traffic system (ref. 1). It ranges from single-pilot, single-engine, private airplanes to multi-crew, multi-engine corporate airplanes to helicopters and sailplanes. A particular example is the small private airplane which is operated in the same weather conditions and under the same air traffic control (ATC) rules as commercial aircraft, but which has less sophisticated avionics and a single pilot with a high workload and perhaps limited proficiency in IFR operations.

Recognizing the size and importance of the GA community, NASA has a continuing emphasis on GA, including aerodynamics, avionics, and flight management. An objective of the research is to decrease the pilot's workload and increase the safety of and capability for IFR flight operations. A useful research tool is the Langley general aviation simulation facility, which can simulate a single-pilot IFR mission scenario from takeoff to landing.

In a recent study pilots flew a series of basic flight maneuvers in the simulator, while control inputs and state variables were recorded. In addition, an oculometer (ref. 2) was used to measure and record the pilot's lookpoint during simulated instrument flight. The objective of the study was to obtain data for refining a time/motion analysis model of single-pilot IFR flight (ref. 3), and also to provide a baseline for comparing results from later studies of advanced avionics.

This report explores the pilot visual scanning behavior during the simulation, and suggests areas for further study in cockpit instrumentation and visual scanning measurements.

SYMBOLS AND ABBREVIATIONS

Symbols

μ mean of normal distribution approximating duty cycle distribution

σ standard deviation of normal distribution approximating duty cycle distribution, dimensionless

x^2 chi-square value computed in goodness-of-fit test, dimensionless

$x^2_{.05}$ critical value of x^2 at .05 significance level

Abbreviations

GA General Aviation

IFR Instrument flight rules

ILS Instrument landing system

VLDS Visual landing display system

VOR Very high frequency omnirange

SIMULATION FACILITY AND EQUIPMENT

The simulation facility incorporated four separate pieces of equipment: a digital computer, a simulated general aviation aircraft cockpit, a visual landing display system (VLDS), and an oculometer system.

Computer

All components of the real-time simulation were linked by a Control Data Cyber 175 computer operating at 32 iterations per second. The main program controlled the flow of calculations and real-time sequencing. Subprograms included equations of motion, aerodynamics, power plant, landing gear and braking, navigation aids (including VOR and ILS in the Atlanta, Georgia area), VLDS drive signals, visibility and ceiling, and data recording. The simulated airplane typified a single-engine, high-wing GA airplane.

Data from the simulation were recorded on magnetic tape for postprocessing. Pilot control inputs and oculometer output values were recorded 32 times per second (every iteration). Another 20 variables including aircraft position and velocities and instrument readings, were recorded twice per second.

Cockpit

The fixed-base simulator cockpit (fig. 1) was arranged so that it could be operated either as a single or twin engine airplane, but for this study a single engine configuration was used. Flight controls included control wheel and column with a hydraulically-driven force-feel system, rudder pedals, throttle, and a switch for electrically operated flaps. Trim controls were provided for pitch and roll. Audio cues were provided for engine and airstream noises. Reference 4 presents a more complete description of the simulator and its validation.

Flight instruments (fig. 2) were representative of those found in general aviation airplanes equipped for instrument flight. Dual navigation and communications radios and transponder were simulated. Fuel and engine instruments were functional.

The forward visual scene was presented on a color TV monitor that was viewed through an optical system which produced a virtual image of the scene focused at infinity. Total field of view was 36 degrees vertically by 48 degrees laterally. No peripheral scene was provided. Between the VLDS and the TV monitor the television signal was processed by a special purpose video mixer which was controlled by the computer to fade out portions of the picture as a function of aircraft position and simulated visibility and ceiling. For this study 1 mile visibility and 76m (250 ft) ceiling were simulated.

VLDS

The terrain model of the VLDS (fig. 3) was at a scale of 1:750, which provided a visual scene of 13.8 by 4.5 kilometers and a maximum altitude of 0.9 km. A standard 510 line color TV camera was positioned over the terrain model in response to computer commands so that the optical head system was at the scaled position of the aircraft. The optical head rotated in pitch, roll, and yaw to present the changing angular relationships that the pilot would see out the window. Reference 5 presents a detailed description of the VLDS and its capabilities.

Oculometer

There are two primary oculometer subsystems: the electro-optical and the signal processing. A filtered incandescent lamp in the electro-optical system generates a beam of red light which is directed toward the subject's eye. Reflections from the eye pass through a beamsplitter to an infrared-sensitive TV camera. The high reflectivity of the human retina for infrared leads to a backlighting of the pupil, so that the camera sees the pupil of the eye as a bright, circular area (fig. 4). It also sees a small bright spot due to reflection at the corneal surface. The relative positions of the center of the pupil and the corneal reflection depend on the angle of rotation of the eyeball with respect to the infrared beam. The signal processing unit operates on the signal from the TV camera to compute this angle of rotation and the coordinates of the lookpoint on, for instance, an instrument panel. The output of the signal processor is a set of calibrated analog signals representing the subject's lookpoint coordinates and pupil diameter.

These analog signals were sent to the computer where they were digitized and recorded. Reference 6 presents a more detailed description of the oculometer system.

TESTS

Three pilots flew nine different flight maneuvers (runs) in the GA simulator. Each pilot flew each run three times. The runs were chosen to represent those which might occur during parts of a flight, and which taken together, could represent a flight profile. This approach is consistent with the Timeline Analysis Program (ref. 3) which is a time-motion model of the pilot's activities during a GA IFR flight. Another reason for this approach is to permit correlation of visual scanning behavior with specific flight activity. The nine maneuvers (runs) flown are listed in Table 1. As shown in Table 1, most of the runs were divided into phases, determined either by pilot callout or computer readout. This division was useful for analyzing specific portions of a run which had unique flight conditions or pilot tasks.

Runs 1-6

Runs 1-6 involved straight and level flight (S&L), climbs, descents, and turns. All runs began at 914m (3000 ft) altitude and 91 knots (105 mph) airspeed. Because of the assumed 76m (250 ft) ceiling, the visual scene was washed out as if by fog or clouds, so all maneuvers were performed on instruments. Climbs and descents involved 305m (1000 ft) altitude change; pilots were instructed to perform them in their usual manner. The climb and descent (runs 2 and 5) were divided into three phases: (1) beginning climb (descent); (2) stabilized climb (descent); and (3) level off. Runs 3, 4 and 6 involved standard rate turns (3 deg/sec) through 180 deg. heading change. Pilots were instructed to make callouts at predesignated conditions, as shown in Table 1.

Run 7

The VOR navigation task was similar to the level turn task (run 4) except that a 30° heading change was made to intercept the radial of a simulated VOR beacon. The pilot made callouts when he intersected the radial and when he was tracking satisfactorily.

Run 8

Run 8 was a holding pattern near a simulated intersection as illustrated in figure 5. The intersection was defined by the Norcross VOR 254° radial and the Atlanta VOR 360° radial. The run began with the airplane outbound on the 360° radial and recording began when the airplane crossed the intersection, and ended after completing the pattern. Altitude was 914m (3000 ft) so the pilot had to rely on instruments and stopwatch to fly the pattern.

Run 9

Run 9 began with the airplane at 853m (2300 ft) altitude on a heading of 120^{0}, preparing to intercept the ILS localizer for runway 8 at the Hartsfield International Airport in Atlanta, Georgia (fig. 5). The run was recorded from intercepting the localizer until touchdown. During phase 97 the pilot transitioned from instruments to the outside scene as the airplane descended below the 76m (250 ft) ceiling.

PILOTS

Three instrument rated pilots participated in the study. Their flying experience, which is summarized in Table 2, ranged from minimal to extensive. Each pilot flew each of the nine test maneuvers three times.

TABLE 2

Background of Subjects

Pilot	A	B	C
Years flying experience	3	12	36
Total no. of hours	225	1700	2300
Rating:			
private	✓	✓	✓
commercial		✓	✓
instrument	✓	✓	✓
single-engine	✓	✓	✓
multi-engine		✓	✓
instructor		✓	✓
No. of IFR flight hours	18	230	280

DATA ANALYSIS

Method of Analysis

The large amount of data recorded makes extensive analysis possible. However, an important feature of this study was the use of the oculometer to measure the pilot's scan pattern, so the analysis concentrated on these data. The following analysis was performed on the data from each run and phase:

1. Computation of instrument-to-instrument probability transition matrices. The elements of these matrices provide a measure of the probability of transitioning from one instrument to another and the probability of remaining on the same instrument. A more detailed discussion is provided in reference 2.

2. Computation of the frequency distribution of dwell time (duration of fixation), including mean and quartiles (intervals containing one-fourth of the frequency distribution) for each instrument.

3. Computation of the frequency distribution of duty cycle, as defined below. Duty cycle was included in the data analysis as part of a continued effort to develop parameters for relating and predicting visual performance.

Dwell time and duty cycle are related as follows:

1. Let n denote the number of fixations on a particular instrument during a phase or run.

2. Let t_i represent the duration (dwell time) of the ith fixation on the instrument.

3. Let y_i represent the time from the start of the ith fixation to the start of the next (i + 1) fixation. Thus, y_i includes the dwell time plus the time spent looking at other instruments before returning. For n fixations only n - 1 values of y are available. In fact, in case of data loss, still fewer values of y might be available, as discussed in the following section.

The duty cycle for the ith fixation is

$$\frac{t_i}{y_i}$$

and the mean duty cycle is

$$\frac{1}{n-1}\sum_{i=1}^{n-1}\left(t_i/y_i\right) \text{ and } y_i > t_i > 0$$

The mean dwell time is

$$\frac{1}{n}\sum_{i=1}^{n} t_i$$

and the percent dwell time is

$$\frac{\sum_{i=1}^{n} t_i}{T}$$

where T is the total length of the run or phase.

Effect Of Data Interruption

Occasionally the oculometer would be unable to determine where the pilot was looking, and the flow of data would be interrupted.

This could happen while the eye was closed during a blink, if the pilot moved his head so his eye translated out of the pickup volume, if he looked at a point far outside the oculometer field of view (such as radios and flight controls), or because of hardware or software malfunction. Data analysis following an interruption depended upon the length of the interruption.

1. 1-3 iterations - If data was interrupted for 3/32 sec. or less, processing continued using the last available point of regard (location of fixation point).

2. 4-11 iterations - 4/32 sec. to 11/32 sec. is the time required for a "blink", so an interruption of this length was assumed to be a blink, and processing resumed using the last available point of regard.

3. 12 or more iterations - If the interruption lasted 12/32 sec. or longer a data error was assumed, and transition and duty cycle calculations restarted with the next successful track.

Table 3 presents the fraction of time in which the oculometer successfully tracked for each run flown. For example, the first replication of run 1 by pilot A lasted 55.0 seconds. During the run the oculometer was tracking for 54.1 seconds.

There were two situations in which the oculometer could be tracking, but uncertain of the instrument being regarded. One occurred because the oculometer field of view was slightly larger than the instrument boundaries, so it would maintain track for a short time when the pilot started to look away. The second occurred because of a criterion in postprocessing that required three or more consecutive iterations (.1 sec.) on the same instrument to be counted as a "dwell"; when only one or two iterations occurred it was assumed to result from sampling during a transition between instruments. Table 4 presents the percent of iterations in track in which a dwell on an instrument was determined. Pilot B's data from run 9 was not analyzed, because of a calibration error which was found after the study was completed.

RESULTS

Percent Time on Instrument

Table 5 presents the percent time on instruments found for each task. The data are averaged over all three runs for the three pilots, except for run 9 (pilot B omitted). A dash (-) in Table 5 signifies that no fixation occurred; a zero (0) indicates that the percent of time on instrument was less than .05 percent.

The pilot never looked at the tachometer in any of the runs (Table 1). The ADF, marker beacon, and DME were used little because none of the runs required the pilot to obtain information from these instruments. Run 8 required two VOR indicators to determine the itersection for initiating the holding pattern; VOR 2 was not needed in other runs. The altimeter and rate-of-climb indicator (IVSI) had moderate usage (4-10 percent and 1-3 percent, respectively) in all runs with no obvious trends of usage.

The out-the-window scene was presented only in phase 97 of run 9, so the percent of time shown in Table 5 may be misleading. The total accumulated time looking out the window was 21.8 seconds of the 1356 seconds in run 9 (1.6 percent). However, 20.9 seconds occurred during 36.0 seconds of phase 97.

The artificial horizon and directional gyro were located directly in front of the pilot, and he spent much of the time looking at them in all runs. The other three instruments--airspeed, turn and bank indicator, and VOR 1--had small to moderate usage, depending upon the task flown. Runs 7, 8, and 9 involved tracking a VOR radial or ILS signal, and VOR 1 was used extensively only in these runs. Runs 3, 4, 6 and 8 involved heading changes and standard rate turns, so the turn and bank indicator was used extensively in these runs and very little in others. The airspeed indicator was used in all runs, with higher usage in runs 2, 3, 5, and 6 which involved controlling airspeed during a climb or descent. The instrument scan patterns used by the pilots are discussed in a later section.

ILS Approach (Run 9)

The simulated ILS approach task (run 9) was analyzed first, because this is one of the most critical areas of aviation operations. The runs were analyzed in two parts - tracking the glide slope (phases 95 and 96), and intercepting the localizer and glide slope (phases 91-93). Phase 97, approach to touchdown, was omitted because much of the phase was flown looking out the window instead of at the instruments.

Transition Matrix

Table 6 presents the probability transition matrices for pilots A and C in phases 95 and 96, and the mean dwell time in seconds. The transition matrices are based on the time on instruments, and are averaged over the three replications. Matrix element a_{ij} represents the probability that the pilot will change his point of regard from the instrument in row i to the instrument in column j. For example, table 6 shows that the probability of transitioning from the artifical horizon to the directional gyro is .013. The column sum is the percent of run time spent looking at the instrument. Table 6 shows that only a small percent of time was spent on the airspeed indicator and altimeter. The pilots spent over 90 percent of the time on three instruments: the artificial horizon, the directional gyro (HSI), and VOR #1, which displayed localizer and glide slope error.

The instrument panel arrangement in the simulator was consistent with the general practice of grouping major flight instruments in a "T" pattern (reference 7). However, the VOR indicator was outside this group. In more sophisticated avionics the course deviation information is often combined in the attitude indicator or horizontal situation indicator. Investigation of the effect of moving the ILS and glide slope information (VOR #1) to a "better" location was beyond the scope of this study.

Table 7 presents the probability transition matrix and mean dwell time for pilots A and C in phases 91-93. Despite the differences in task, the transition matrix in Table 7 is very similiar to the matrix for phases 95-96 in Table 6. The artificial horizon, directional gyro and VOR indicator were still the dominant instruments.

Histograms

To try to get a better understanding of the pilots' scanning behavior, the dwell time and duty cycle data for the directional gyro, artificial horizon, and VOR/ILS indicator were examined in more detail. Initial analysis concentrated on pilot C in phases 95 and 96.

Figure 6 shows the distribution of dwell time occurrences for the directional gyro in phases 95-96. The distribution appears to be bimodal, with one mode at 3-5 iterations (.1 - .2 sec) and another mode at 15-25 iterations (.5 - .8 sec). It seems reasonable that at the second mode the pilot would have sufficient time to assimilate data, but the first mode with the very short dwell times is puzzling. One hypothesis is that the first mode does not involve data transfer, but is an artifact resulting from the directional gyro being at the center of the pilot's scan pattern. If true, then (1) it gives an indication of the center of the pilot's scan pattern, (2) other instruments should not show the mode at short dwell time, and (3) the data in the first mode could be omitted in analyzing data transfer. Omitting the short (less than 10 iterations) dwell times the data had .25, .50, and .75 percent quartiles at:

.25 quartile = (.50 sec)
.50 quartile = (.66 sec)
.75 quartile = (.78 sec)

Thus, despite the data's lack of form and the occasional long dwell times, the majority of the dwell times on the directional gyro fell in a relatively small interval.

Figure 7 shows the distribution of dwell time for the artificial horizon and the VOR instrument. Neither distribution shows the large occurrence of short dwell times seen with the directional gyro (fig. 6). Therefore, in analyzing these duty cycles, all of the data were used.

Figure 8 shows the duty cycle data for the directional gyro in phases 95-96. Each point represents a look at the instrument by pilot C. The only obvious pattern is a relatively large number of occurrences at short dwell times. These correspond to the peak at short dwell times in figure 6.

Figure 9 shows the distribution of the duty cycle data with dwell times less than .3 second (10 iterations) omitted. Figure 9 is interesting in that it resembles a normal distribution except for the lack of a tail on the left side. If the duty cycle data were distributed normally, then it might provide another basis for examining and predicting visual scan characteristics.

Figure 10 shows the same distribution plotted on probability paper. If the distribution were normal, the histogram would plot as a straight line. Figure 10 is straight over much of the histogram indicating the duty cycle distribution may be approximated by a normal population with mean μ and standard deviation σ. The mean is estimated by the median $X_{.50}$ since the mean and median of a normal distribution are equal. In figure 10

$\mu = X_{.50} = .505.$

The standard deviation is estimated by relating the duty cycle variable X to a standard normal variable Z, having mean zero and standard deviation of one. The values of X and Z corresponding to a cumulative probability p are denoted X_p and Z_p, respectively, and are related by

$$Z_p = \frac{X_p - \mu}{\sigma}$$

The cumulative probability p is the area under the standard normal curve from $-\infty$ to Z_p, and is available in statistical tables (ref. 8, 9). At any selected cumulative probability, Z_p can be used to compute σ by

$$\sigma = \frac{X_p - \mu}{Z_p}$$

For example, 40 percent of the area under the normal curve lies between $Z_{.50} = 0$ and $Z_{.90} = 1.283$. From figure 10, 40 percent of the duty cycle population lies between $X_{.50} = \mu = .505$ and $X_{.90} = .710$. Therefore,

$$Z_{.90} = 1.283 = \frac{X_{.90} - \mu}{\sigma} = \frac{(.710 - .505)}{\sigma}$$

and

$$\sigma = \frac{.205}{1.283} = .160$$

Figure 11 shows the duty cycle histograms for the artificial horizon and the VOR indicator, plotted on probability paper. Both curves show a straight-line fit for the data over much of the histogram, but over a smaller range than for the directional gyro in figure 10. This suggests a normal distribution, but probably a poorer fit than the directional gyro data.

The next step was to examine the duty cycle data (1) for the same pilot performing a different task, and (2) a different pilot.

Figure 12 shows the duty cycle histograms for pilot C in phases 91-93 (intercepting the localizer and glide slope). Figure 12 shows essentially the same trends as figures 10-11, indicating that the duty cycle values might be approximated over much of the range by a normal curve centered at the median.

The duty cycle data for pilot A was analyzed next. Figures 13 and 14 show the duty cycle histograms for pilot A in phases 95-96 and 91-93, respectively. The curves are similar to figures 10-12 for pilot C, each having a region of linearity with nonlinearity near the ends. The requirement that all duty cycle data must lie in the interval 0.-1.0 forces the curves to be non-linear at both ends. This corresponds to cutting off the tail of the normal curve. Also, if the median is large or small the duty cycle distribution will be skewed, resulting in a poor approximation to a normal curve.

Duty Cycle Summary

Since figures 10-12 suggest a normal distribution for some of the duty cycle data, a chi-square goodness of fit test (reference 8) was made to test the hypothesis that a normal curve approximates the duty cycle distribution. The value of X^2 is computed as

$$X^2 = \sum_{j=1}^{k} (o_j - e_j)^2/e_j$$

where o_j is the observed (experimental) frequency, e_j is the expected (theoretical) frequency, N is the total frequency, and

$$\sum o_j = \sum e_j = N$$

If the data actually come from a normal distribution, then theoretical χ^2 distribution is followed with (K-3) degrees of freedom, where K is the number of classes (intervals) used in computing χ^2.

Testing at the .05 significance level, with critical value $\chi^2_{.05}$, the hypothesis of normal distribution of the data would be rejected if $\chi^2 > \chi^2_{.05}$.

Table 8 summarizes the duty cycle data for both pilots in both tasks (phases 91-93 and 95-96). In all cases the duty cycle data for the directional gyro appeared to correlate with a normal distribution with mean μ and standard deviation σ. The hypothesis of normality was generally rejected for the other two instruments, probably because of skewness in the distribution.

In addition to the distribution of the duty cycle data, its consistency (or inconsistency) is important. Table 8 shows that for the artificial horizon and the directional gyro the duty cycle distribution (μ and σ) was essentially the same in both phases for pilot A. The duty cycle distribution was also the same in both phases for pilot C. However, the statistics were different between the two pilots, suggesting that the pilots scanned the instruments differently.

The median cycle for the VOR/ILS indicator was different between pilots and tasks (phases). This is reasonable because the indicator was used differently in the two tasks--for lateral (localizer) guidance in phases 91-93, and for lateral and vertical (glide slope) guidance in phases 95-96.

Duty cycle, then, shows characteristics desirable in a scanning behavior metric--an appreciable change with different scan patterns, an appreciable change with change in visual task, and consistency with a repeated task.

Dwell Time Summary

Tables 9 and 10 present the mean and quartiles of dwell (fixation) time for each pilot, based on the dwell times which occurred as part of a duty cycle. Table 9 shows the data for phases 91-93; Table 10 shows the data for phases 95-96. The tachometer, ADF, and window are omitted from the tables because neither pilot looked at them at any time. Quartile data is presented for those instruments having at least 12 duty cycle occurrences. When a duty cycle was interrupted by the oculometer losing track, the postprocessing program would drop the previous value of dwell for each instrument and start over when tracking resumed. Therefore, the data is based on fewer samples of dwell than the mean dwell time shown in Tables 6 and 7, which is based on the probability transition matrix.

Tables 9 and 10 show that pilot A had considerably longer dwell time on the artificial horizon than pilot C, and shorter dwell time on the directional gyro. This is the same trend as the duty cycle data in Table 8. Since duty cycle is equal to the dwell time divided by the time between fixations, the data in Tables 8-10 were used to compute the time between fixations, and the results are presented in Table 11. The time between fixations appears similar for the artificial horizon and directional gyro, and suggests frequent sampling --about once every 1.3 second. The VOR indicator data are unequal, which would be expected because of the difference in the task in the two phases, and indicate a much longer period between fixations.

Dwell Time and Duty Cycle in Runs 1-8

Table 12 summarizes the dwell time and duty cycle data for all three pilots in runs 1-8. The table generally shows consistency between runs in both dwell time and duty cycle. In most cases the median dwell time and the mean dwell time are close, with the mean dwell time being larger because of the occasional occurrence of long dwell times. In the case of the artificial horizon, the difference tends to be about 0.3 second. As indicated by the quartile data, over 25 percent of all the looks at the artificial horizon lasted over one second. For example, in run 1, 67 of the 224 dwell occurrences lasted over one second; and 22 of these 67 lasted over two seconds. It seems reasonable that pitch and roll attitude could be checked quickly, but a longer fixation period would be necessary to determine the rate of change of attitude. Work is presently underway to relate scanning data to manual activities.

There is no apparent correlation in Table 12 between dwell time and duty cycle. They show different aspects of the visual scan process. Together they may provide insight into the pilot's information requirements. It appears reasonable that dwell time is an indicator of the time required to extract information from an instrument. This is consistent with the relatively short dwell times for the marker beacon indicator light and the IVSI, and the longer dwell time for the turn and bank indicator and the altimeter. If this is true, then duty cycle may be an indicator of how often the pilot needs the information. The low duty cycle for the airspeed indicator and IVSI in table 12 suggests a low sampling frequency (relatively long time between fixations) for these instruments. Together, dwell time and duty cycle may both provide useful data for developing mathematical models of pilot scanning behavior.

Scan Pattern

The probability transformation matrix can provide insight into the pilot's visual scan pattern. It is frequently assumed that a pilot will use a sequential instrument scan pattern--looking at several instruments before returning to the original instrument. However, previous studies (ref. 2, 6, 10) of scan patterns during simulated approaches in commercial aircraft indicated that pilots tended to "home" on one instrument and then transition directly between the "home" position and another instrument, rather than scanning several instruments before returning.

Table 13 presents a form of the transition matrix for runs 1-8. The matrix is in terms of total number of occurrences rather than transition probability, as was presented in Tables 6 and 7. The probability transition matrix can be obtained by dividing the matrix by the total number of intervals (15321 for run 1). A value on the main diagonal represents the total number of 1/32 second intervals in which the pilot viewed the particular instrument, in all nine replications (three by each pilot). The off-diagonal terms are the number of transitions from the instrument indicated at the side of the matrix, to the instrument indicated at the top. For example, Table 20a shows 152 transitions from the directional gyro to the artificial horizon in run 1, and 147 transitions from the artificial horizon to the directional gyro.

Table 20 shows two important characteristics. First, a high percentage of the transitions were either to or from the artificial horizon. This was 448 of the 584 transitions in run 1 (Table 20a). This indicates that the pilots used the artificial horizon as "home" and that most transitions were to one instrument and then back. Second, the transpose elements of the matrix tend to be equal, showing no obvious pattern for a sequence of transitions. Occasionally, two or more instruments were scanned before the pilot returned to the artificial horizon, but there was no discernible pattern.

This result suggests that a more efficient presentation might combine the information to be presented into fewer instruments. This could increase the dwell time, because the pilot might need more time to assimilate the information; but fewer transitions would be required, so the duty cycle might actually decrease. This will be tested in future simulation studies.

CONCLUDING REMARKS

A simulation of tasks associated with single pilot general aviation flight under instrument flight rules has been conducted as a baseline for future research studies on advanced flight controls and avionics. During the simulation the pilot's visual scan pattern including point of regard was measured and recorded. Analysis of the visual scan data indicates:

1. Except for the artificial horizon, located directly in front of the pilot, the number of occurrences of dwell ("looks") and the dwell time (duration) were consistent with tasks information requirements, and appear related to the time required to assimilate data from an instrument.

2. A second parameter, duty cycle, was investigated for the first time in this study. Like dwell time, it tended to be different between instruments but consistent between runs. Statistical analysis indicated that skewness prevented the duty cycle distribution for an instrument from approximating a normal distribution.

3. Dwell time and duty cycle together may provide an indication of instrument sampling duration and frequency, which may be useful in modeling visual scanning behavior.

4. Analysis of the transitions between instruments showed that pilots tended to transition from a primary instrument (the artificial horizon) to another instrument and then return, rather than scanning a sequence of instruments.

REFERENCES

1. Annual Review of Aircraft Accident Data, Calendar Year 1978, NTSB-ARG-78-1.
2. Waller, Marvin C.: and Wise, Marion A.: The Oculometer in Flight Management Research. AIAA Paper 75-107, 1975.
3. Hinton, David A.; and Shaughnessy, John D.: Adaption of Time Line Analysis Program to Single Pilot Instrument Flight Research. NASA Technical Memorandum 78478. August 1978.
4. Harris, Randall L., Sr.: Validation of a Research Simulator for Light Aircraft Approach and Landing. Presented at the 1975 SAE National Business Aircraft Meeting, April 8-11, 1975.
5. Rollins, John D.: Description and Performance of the Langley Visual Landing Display System. NASA TM 78742, August 1978.
6. Spady, Amos A., Jr.: Airline Pilot Scan Patterns During Simulated ILS Approaches. NASA TP-1250, 1978.
7. Ontiveros, Robert J.; Spangler, Roman M.; and Sulzer, Richard L.: General Aviation (FAR 23) Cockpit Standardization Analysis. Federal Aviation Administration FAA-RD-77-192, March 1978.
8. Snedicor, George W.; and Cockran, William G.: Statistical Methods. Sixth ed., Iowa State University Press, 1968.
9. Hoel, Paul G.: Introduction to Mathematical Statistics. Fourth ed., John Wiley and Sons, 1971.
10. Weir, David H.; and Klein, Richard H.: The Measurement and Analysis of Pilot Scanning and Control Behavior During Simulated Instrument Approaches. NASA CR-1535, June 1970.

TABLE 1

Simulated Flight Tasks

Run	Title	Phase	Description	Pilot Callout
1	Straight & Level		Straight & level flight recorded for 1 minute	. established in S&L
2	Climb	21	Transition from S&L to climb	. entering climb
		22	Established in climb	. maintaining climb
		23	Transition to S&L	. leveling off
				. in level flight
3	Climbing turn		Record during time from turn entry to exit	. entering turn
				. out of turn
4	Level turn		Similar to run 3	
6	Descending turn		Similar to run 3	
5	Descent	51	Transition from S&L to descent	. entering descent
		52	Established in descent	. maintaining descent
		53	Transition to S&L	. leveling off
				. in level flight
7	VOR navigation	71	Record from radial intercept until tracking	. intercepting radial
		72	Record 1 minute of radial tracking	. tracking radial
8	Holding pattern	81	From approach to passing intersection	. approaching intersection
		82	Past intersection, on entry leg prior to turn	. past intersection
		83	Energy turn and intercept	. beginning entry turn
		84	Turn away from radial	. beginning turn away from radia
		85	Leg off radial	. on outbound leg

[illegible]	Title	Phase	Description	Pilot Callout
		86	Turn towards radial	. beginning turn toward radial
		87	Leg on radial	. inbound on radial
				. beginning turn away from radial
9	ILS Approach	91	Approach and intercept localizer	. approaching localizer
		92	Track localizer	. on localizer
		93	Pass outer marker and intercept glide slope	. outer marker
		94	Track glide slope in first 3rd of distance to middle marker*	*fraction of distance between LOM and MM were read out from computer
		95	Track glide slope in second 3rd of distance to MM	
		96	Track glide slope in final 3rd of distance to MM	
		97	Cross MM and continue to touchdown	. middle marker

TABLE 3.- FRACTION OF RUN TIME WITH SUCCESSFUL OCULOMETER TRACKING

Run No.	Pilot A Replications			Pilot B Replications			Pilot C Replications		
1	54.1/55.0	60.7/62.0	55.7/60.5	56.0/67.5	57.0/61.0	49.2/60.0	50.5/63.5	49.0/64.5	56.3/63.5
2	120.0/126.5	132.5/139.5	116.4/124.0	124.9/162.0	113.0/139.0	103.4/131.5	135.6/150.0	117.2/123.0	135.7/156.5
3	52.7/56.0	68.9/70.5	64.8/65.5	64.1/70.5	55.5/62.5	61.3/73.0	51.4/55.5	52.1/55.0	50.1/52.5
4	49.6/53.5	47.3/49.0	62.7/65.0	72.4/77.0	66.8/76.0	61.9/81.0	47.0/54.5	51.3/58.5	62.7/66.0
5	133.6/156.5	124.3/144.0	132.0/150.0	166.2/195.0	136.6/176.0	103.2/140.5	109.7/131.5	104.6/116.5	112.9/131.5
6	53.8/60.5	61.8/70.5	60.7/62.0	70.9/79.0	53.9/55.5	65.4/79.5	53.5/68.0	58.1/59.0	41.6/51.0
7	183.2/205.5	198.2/211.0	194.9/209.5	219.1/246.0	236.3/256.0	183.4/257.5	167.9/228.5	189.9/243.0	191.0/201.0
8	428.1/535.5	426.2/492.5	473.9/540.0	448.9/534.0	499.2/567.0	471.5/533.5	339.5/472.5	302.2/489.0	321.9/476.0
9	258.3/308.5	259.3/315.5	256.4/314.5	268.7/340.5	295.0/342.5	306.0/342.5	195.4/294.5	227.0/328.0	235.2/325.5

TABLE 5.- PERCENT TIME ON INSTRUMENT FOR ALL PILOTS

Cockpit Instrument	Run Number (described in Table 1) 1	2	3	4	5	6	7	8	9
Tachometer	-	-	-	-	-	-	-	-	-
ADF	0	0.1	0.2	0.1	0.1	0	0	0	0.2
Marker Bcn.	0	0	-	2.4	0	0	0.1	0.1	0
Altimeter	10.6	9.4	4.1	6.7	9.2	3.9	8.1	6.1	3.2
Artificial Horizon	58.7	64.3	59.7	62.7	67.0	61.5	63.3	56.5	42.4
Airspeed	1.3	2.8	2.9	1.5	2.9	5.1	1.5	1.7	1.2
IVSI	1.7	2.8	1.3	0.4	2.1	2.5	1.9	1.6	1.2
Dir. Gyro.	25.4	19.7	17.6	11.9	17.9	13.7	18.9	18.9	31.7
Turn & Bank	0.9	0.8	14.0	14.3	0.6	12.8	0.8	4.3	0.5
VOR 1	0.1	0	-	0	0.1	0.3	4.9	4.6	17.0
DME	1.0	0.1	0	0	0.1	-	0.4	0.7	1.1
VOR 2	0.1	0	0.2	0.1	0	-	0.2	5.5	0
Window	-	0	-	-	-	-	-	0	1.6

TABLE 4.- PERCENT OF TIME IN TRACK IN WHICH A DWELL ON INSTRUMENT WAS DETERMINED

Run No.	Pilot A Replications			Pilot B Replications			Pilot C Replications		
1	97.6	99.2	98.0	93.8	97.2	94.1	99.3	97.7	98.1
2	96.9	98.2	97.7	96.0	93.7	95.3	97.5	96.3	95.6
3	97.3	98.1	95.0	94.4	94.7	93.8	97.0	93.5	96.1
4	97.2	98.1	87.1	90.6	94.9	93.5	94.6	89.4	97.1
5	96.7	97.7	97.8	91.4	93.9	94.7	98.2	93.9	95.7
6	96.2	97.2	96.4	94.6	95.4	92.9	90.2	95.4	95.6
7	95.9	97.8	90.8	91.4	90.7	94.6	92.0	83.5	74.3
8	94.4	96.8	93.3	89.6	88.4	92.9	91.6	88.3	84.8
9	92.6	96.0	96.1	--	--	--	92.0	93.7	90.3

PROBABILITY TRANSFORMATION MATRIX

	TACH	ADF	WINDOW	MKR BCN	ALT	ART HOR	AIRSPD	IVSI	DR GYRO	TRN BNK	VOR 1	DME	VOR 2
TACH	0.000	0.000	0.000	0.000	0.000	0.000	0.000	0.000	0.000	0.000	0.000	0.000	0.000
ADF	0.000	.061	0.000	0.000	.000	0.000	0.000	.000	0.000	0.000	0.000	0.000	0.000
WINDOW	0.000	0.000	.061	0.000	0.000	.000	0.000	0.000	0.000	0.000	0.000	0.000	0.000
MKR BCN	0.000	0.000	0.000	.000	0.000	0.000	0.000	0.000	0.000	0.000	0.000	0.000	0.000
ALT	0.000	.000	0.000	.000	.029	.002	0.000	.000	.000	0.000	.000	0.000	0.000
ART HOR	0.000	0.000	.000	0.000	.002	.396	.000	.000	.013	.000	.004	.000	0.000
AIRSPD	0.000	0.000	0.000	0.000	0.000	.001	.010	0.000	.000	.000	.000	0.000	0.000
IVSI	0.000	0.000	0.000	0.000	.000	.000	.000	.011	.000	0.000	.000	0.000	0.000
DR GYRO	0.000	0.000	0.000	0.000	.000	.014	.000	.001	.312	0.000	.004	.002	0.000
TRN BNK	0.000	0.000	0.000	0.000	0.000	.000	.000	0.000	.000	.002	0.000	0.000	0.000
VOR 1	0.000	0.000	0.000	0.000	0.000	.003	.000	.000	.007	.000	.170	.000	0.000
DME	0.000	0.000	0.000	0.000	0.000	.000	0.000	0.000	.000	0.000	.002	.010	0.000
VOR 2	0.000	0.000	0.000	0.000	0.000	0.000	0.000	0.000	0.000	0.000	0.000	0.000	0.000
MEAN DWELL (COUNTS)	0.0	24.0	22.0	7.0	13.8	21.4	18.1	8.2	16.2	7.8	17.7	5.5	0.0
(SEC)	0.000	.750	.688	.219	.430	.668	.565	.257	.507	.244	.554	.173	0.000

Table 6. Probability Transformation Matrix, Pilots A and C, Phases 95-96.

PROBABILITY TRANSFORMATION MATRIX

	TACH	ADF	WINDOW	MKR BCN	ALT	ART HOR	AIRSPD	IVSI	DR GYRO	TRN BNK	VOR 1	DME	VOR 2
TACH	0.000	0.000	0.000	0.000	0.000	0.000	0.000	0.000	0.000	0.000	0.000	0.000	0.000
ADF	0.000	.002	0.000	0.000	.000	0.000	0.000	.000	.060	0.000	.000	0.000	0.000
WINDOW	0.000	0.000	.000	0.000	0.000	.000	0.000	0.000	0.000	0.000	0.000	0.000	0.000
MKR BCN	0.000	0.000	0.000	.001	0.000	.000	0.000	0.000	0.000	0.000	0.000	0.000	0.000
ALT	0.000	0.000	0.000	0.000	.033	.001	0.000	.000	.000	0.000	.000	0.000	0.000
ART HOR	0.060	.000	0.000	.000	.002	.399	.001	.000	.011	.000	.063	.000	0.000
AIRSPD	0.000	0.000	0.000	0.000	0.000	.001	.008	0.000	.000	.000	0.000	0.000	0.000
IVSI	0.000	0.000	0.000	0.000	.000	.001	0.000	.014	.001	.000	.031	.000	0.000
DR GYRO	0.000	.000	.000	0.000	.000	.012	.000	.001	.309	.000	.063	.002	0.000
TRN BNK	0.000	0.000	0.000	0.000	0.000	.000	.000	0.000	.000	.008	0.000	.000	.000
VOR 1	0.000	.000	0.000	0.000	0.000	.002	0.000	.001	.006	0.000	.165	.000	0.000
DME	0.000	0.000	0.000	0.000	0.000	0.000	0.000	0.000	.000	0.000	.032	.009	0.000
VOR 2	0.000	0.000	0.000	0.000	0.000	.000	0.000	0.000	0.000	0.000	0.000	0.000	.000
MEAN DWELL (COUNTS)	0.0	6.6	4.0	10.0	15.5	24.3	12.7	7.6	17.8	16.5	19.9	5.2	5.0
(SEC)	0.000	.206	.125	.313	.494	.760	.398	.237	.556	.516	.621	.164	.156

Table 7. Probability Transformation Matrix, Phases 91-93.

Table 8. - Duty Cycle Data For Run 9

Pilot	A		C	
Phase	91-93	95-96	91-93	95-96
Artificial Horizon				
μ	.480	.480	.302	.309
σ	.235	.212	.219	.207
χ^2	16.2	29.3	20.5	29.5
$\chi^2_{.95}$	26.3	25.0	23.7	21.0
Approximately Normal	Yes	No	Yes	No
Directional Gyro				
μ	.372	.374	.509	.505
σ	.188	.181	.195	.163
χ^2	20.4	8.6	18.1	12.5
$\chi^2_{.95}$	23.7	22.4	25.0	19.7
Approximately Normal	Yes	Yes	Yes	Yes
VOR #1 Indicator				
μ	.100	.135	.208	.228
σ	.170	.171	.226	.200
χ^2	37.9	16.2	20.1	11.2
$\chi^2_{.95}$	16.9	14.1	22.4	19.7
Approximately Normal	No	No	Yes	Yes

Table 9. - Dwell Time Data For Phases 91-93

Instrument	Marker BCN.		Altimeter		Art. Horiz.		Airspeed		IVSI	
Pilot	A	C	A	C	A	C	A	C	A	C
Mean (sec.)			.50	.63	.83	.49	.35		.24	.21
.25 Quartile (counts)			9		13	8			4	
.75 Quartile (counts)			21		28	19			9	
Median (counts)			16		19	13			6	
Median (sec.)			.50		.59	.41			.19	
No. of Occurrences	0	0	17	4	163	92	8	0	18	7

Instrument	Dir. Gyro*		Turn & Bank		VOR 1		DME		VOR 2	
Pilot	A	C	A	C	A	C	A	C	A	C
Mean (sec.)	.60	.82	.19		.51	.62	.13	.15		
.25 Quartile (counts)	14	17			11	12		3		
.75 Quartile (counts)	22	26			21	22		4		
Median (counts)	17	22			14	16		4		
Median (sec.)	.53	.69			.44	.50		.13		
No. of Occurrences	118	65	5	0	52	52	5	23	0	0

* <9 omitted.

Table 10. - Dwell Time Data For Phases 95-96

Instrument	Marker BCN.		Altimeter		Art. Horiz.		Airspeed		IVSI	
Pilot	A	C	A	C	A	C	A	C	A	C
Mean (sec.)		.14	.58	.38	.86	.43	.45	.53	.30	.30
.25 Quartile (counts)				6	13	8				
.75 Quartile (counts)				16	39	18				
Median (counts)				9	19	11				
Median (sec.)				.28	.59	.34				
No. of Occurrences	0	2	7	22	158	185	2	1	3	11

Instrument	Dir. Gyro		Turn & Bank		VOR 1		DME		VOR 2	
Pilot	A	C	A	C	A	C	A	C	A	C
Mean (sec.)	.64	.71	.14		.50	.56	.11	.19	.09	
.25 Quartile (counts)	14	16			12	10		3		
.75 Quartile (counts)	24	25			19	23		6		
Median (counts)	18	21			16	17		5		
Median (sec.)	.56	.66			.50	.53		.16		
No. of Occurrences	118	105	6	0	67	97	3	33	2	0

Table 11. - Time Between Fixations (sec.) Based On Median Dwell Time and Duty Cycle

Pilot	A		C	
Phase	91-93	95-96	91-93	95-96
Artificial Horizon	1.22	1.23	1.36	1.10
Directional Gyro.	1.42	1.50	1.36	1.31
VOR/ILS Indicator	4.4	3.70	2.4	2.32

Table 12. Dwell Time and Duty Cycle Data

(a) Run 1

Instrument	Mkr Bcn.	Alt.	Art. Horiz.	Airspeed	IVSI	Dir. Gyro.	Turn & Bank	VOR 1	DME	VOR 2
Mean Dwell (Sec.)		.58	1.03	.73	.25	.63	.44		.43	
Median Dwell (Sec.)		.50	.53		.13	.62				
.25 Quartile		.38	.44		.16	.47				
.75 Quartile		.66	1.16		.28	.88				
Mean Duty Cycle		.26	.55		.05	.35				
No. of Occurrences	0	63	224	2	11	112	1	0	5	0

(b) Run 2

Instrument	Mkr Bcn.	Alt.	Art. Horiz.	Airspeed	IVSI	Dir. Gyro.	Turn & Bank	VOR 1	DME	VOR 2
Mean Dwell (Sec.)	.53	.43	.31	.51	.36	.64	.44			
Median Dwell (Sec.)		.38	.53	.47	.34	.47				
.25 Quartile		.28	.38	.31	.22	.53				
.75 Quartile		.50	1.12	.63	.47	.75				
Mean Duty Cycle		.13	.52	.08	.07	.28				
No. of Occurrences	1	186	548	26	64	238	3	0	0	0

Table 12. Continued.

(c) Run 3

Instrument	Mkr Bcn.	Alt.	Art. Horiz.	Airspeed	IVSI	Dir. Gyro.	Turn & Bank	VOR 1	DME	VOR 2
Mean Dwell (Sec.)		.42	1.05	.27	.35	.70	.56			.11
Median Dwell (Sec.)		.38	.72	.19		.62	.50			
.25 Quartile		.16	.41	.12		.41	.41			
.75 Quartile		.53	1.28	.34		.91	.66			
Mean Duty Cycle		.10	.54	.14		.37	.20			
No. of Occurrences	0	33	249	30	9	92	99	0	0	2

(d) Run 4

Instrument	Mkr Bcn.	Alt.	Art. Horiz.	Airspeed	IVSI	Dir. Gyro.	Turn & Bank	VOR 1	DME	VOR 2
Mean Dwell (Sec.)	.45	.47	.88	.25	.17	.63	.56			
Median Dwell (Sec.)	.38	.47	.62	.16		.56	.50			
.25 Quartile	.25	.25	.38	.09		.44	.38			
.75 Quartile	.56	.59	1.03	.28		.69	.62			
Mean Duty Cycle	.24	.12	.50	.05		.30	.22			
No. of Occurrences	32	50	268	18	5	67	90	0	0	0

Table 12. Continued.

(e) Run 5

Instrument	Mkr Bcn.	Alt.	Art. Horiz.	Airspeed	IVSI	Dir. Gyro.	Turn & Bank	VOR 1	DME	VOR 2
Mean Dwell (Sec.)	.33	.44	.98	.53	.28	.60	.40	.44	.19	
Median Dwell (Sec.)		.38	.69	.47	.22	.53				
.25 Quartile		.28	.44	.28	.12	.41				
.75 Quartile		.53	1.19	.62	.38	.69				
Mean Duty Cycle		.14	.57	.10	.07	.30				
No. of Occurrences	4	168	531	25	46	200	5	2	3	0

(f) Run 6

Instrument	Mkr Bcn.	Alt.	Art. Horiz.	Airspeed	IVSI	Dir. Gyro.	Turn & Bank	VOR 1	DME	VOR 2
Mean Dwell (Sec.)		.34	1.00	.41	.42	.65	.55	.19		
Median Dwell (Sec.)		.34	.66	.34	.38	.53	.50			
.25 Quartile		.12	.41	.16	.25	.41	.28			
.75 Quartile		.50	1.16	.47	.56	.81	.69			
Mean Duty Cycle		.07	.50	.20	.07	.34	.17			
No. of Occurrences	0	26	240	43	20	64	76	1	0	0

Table 12. Concluded.

(g) Run 7

Instrument	Mkr Bcn.	Alt.	Art. Horiz.	Airspeed	IVSI	Dir. Gyro.	Turn & Bank	VOR 1	DME	VOR 2
Mean Dwell (Sec.)	.24	.48	1.05	.48	.26	.62	.36	.50	.15	.09
Median Dwell (Sec.)	.16	.44	.66	.34	.22	.56	.25	.44	.09	
.25 Quartile	.09	.28	.38	.12	.12	.44	.09	.25	.09	
.75 Quartile	.31	.62	1.19	.50	.34	.72	.31	.66	.16	
Mean Duty Cycle	.10	.09	.54	.08	.04	.33	.05	.10	.03	
No. of Occurrences	10	166	728	14	77	292	11	109	17	2

(h) Run 8

Instrument	Mkr Bcn.	Alt.	Art. Horiz.	Airspeed	IVSI	Dir. Gyro.	Turn & Bank	VOR 1	DME	VOR 2
Mean Dwell (Sec.)	.19	.42	.88	.32	.29	.61	.43	.50	.33	.62
Median Dwell (Sec.)	.16	.41	.59	.22	.22	.53	.44	.41	.19	.56
.25 Quartile	.09	.25	.38	.12	.12	.41	.19	.25	.12	.44
.75 Quartile	.22	.53	1.06	.41	.34	.69	.59	.59	.38	.72
Mean Duty Cycle	.04	.12	.49	.19	.05	.32	.20	.13	.13	.11
No. of Occurrences	12.	298	1671	89	97	662	219	133	63	109

SUMMARY FOR 9 RUNS/PHASES
TRANSFORMATION MATRIX IN TOTAL ITERATIONS

RUN 0

	TACH	ADF	WINDOW	MKR BCN	ALT	ART HOR	AIRSPD	IVSI	DR GYRO	TRN BNK	VOR 1	DME	VOR 2	
TACH	0	0	0	0	0	0	0	0	0	0	0	0	0	
ADF	0	10	0	0	1	1	0	0	0	0	0	0	0	
WINDOW	0	0	0	0	0	0	0	0	0	0	0	0	0	
MKR BCN	0	0	0	4	1	0	0	0	0	0	0	0	0	
ALT	0	2	0	1	1541	70	0	8	12	0	1	0	0	
ART HOR	0	0	0	0	79	8750	9	4	147	4	0	0	0	
AIRSPD	0	0	0	0	0	9	189	0	0	1	0	0	0	
IVSI	0	0	0	0	7	9	0	235	6	0	0	0	1	
DR GYRO	0	0	0	0	7	152	1	10	3709	4	1	6	2	
TRN BNK	0	0	0	0	0	4	2	0	4	130	0	0	0	
VOR 1	0	0	0	0	0	0	0	0	2	0	11	0	0	
DME	0	0	0	0	0	0	0	1	9	0	0	137	0	
VOR 2	0	0	0	0	0	0	0	0	1	1	0	1	21	
TOTAL	0	12	0	5	1636	8995	201	258	3890	140	13	147	24	15321
OCCURRENCES	0	2	0	1	95	245	12	23	181	10	2	10	3	

Table 13. Transition Matrix.

(a) Run 1

SUMMARY FOR 9 RUNS/PHASES
TRANSFORMATION MATRIX IN TOTAL ITERATIONS

RUN 1

	TACH	ADF	WINDOW	MKR BCN	ALT	ART HOR	AIRSPD	IVSI	DR GYRO	TRN BNK	VOR 1	DME	VOR 2	
TACH	0	0	0	0	0	0	0	0	0	0	0	0	0	
ADF	0	45	0	0	5	2	0	0	0	0	0	0	0	
WINDOW	0	0	8	0	0	0	0	0	1	0	0	0	0	
MKR BCN	0	0	0	3	1	0	0	0	0	0	0	0	0	
ALT	0	1	0	0	2970	177	1	30	16	0	0	0	0	
ART HOR	0	5	0	1	173	21273	44	14	366	15	0	1	0	
AIRSPD	0	0	0	0	0	53	887	1	3	2	0	0	0	
IVSI	0	0	0	0	14	43	0	872	21	0	0	0	0	
DR GYRO	0	1	1	0	33	334	8	32	6282	7	0	2	1	
TRN BNK	0	0	0	0	0	10	7	0	7	247	0	0	0	
VOR 1	0	0	0	0	0	0	0	0	1	0	4	0	0	
DME	0	0	0	0	0	0	0	1	1	0	1	17	0	
VOR 2	0	0	0	0	0	0	0	0	0	1	0	0	5	
TOTAL	0	52	9	4	3196	21892	947	950	6698	272	5	20	6	34051
OCCURRENCES	0	7	1	1	226	619	60	78	416	25	1	3	1	

Table 13. Continued.

(b) Run 2

SUMMARY FOR 9 RUNS/PHASES
TRANSFORMATION MATRIX IN TOTAL ITERATIONS

RUN 2

	TACH	ADF	WINDOW	MKR BCN	ALT	ART HOR	AIRSPD	IVSI	DR GYRO	TRN BNK	VOR 1	DME	VOR 2	
TACH	0	0	0	0	0	0	0	0	0	0	0	0	0	
ADF	0	25	0	0	3	2	0	0	0	0	0	0	0	
WINDOW	0	0	0	0	0	0	0	0	0	0	0	0	0	
MKR BCN	0	0	0	0	0	0	0	0	0	0	0	0	0	
ALT	0	4	0	0	608	25	0	9	8	0	0	0	0	
ART HOR	0	1	0	0	34	9256	26	5	126	79	0	1	1	
AIRSPD	0	0	0	0	0	25	417	0	0	15	0	0	0	
IVSI	0	0	0	0	1	10	0	186	6	1	0	0	0	
DR GYRO	0	0	0	0	5	121	1	3	2646	35	0	0	0	
TRN BNK	0	0	0	0	5	90	12	1	21	2109	0	0	1	
VOR 1	0	0	0	0	0	0	0	0	0	0	0	0	0	
DME	0	0	0	0	0	0	0	0	1	0	0	3	0	
VOR 2	0	0	0	0	0	0	0	0	2	0	0	0	22	
TOTAL	0	30	0	0	656	9529	456	204	2810	2239	0	4	24	15952
OCCURRENCES	0	5	0	0	48	273	39	18	164	130	0	1	2	

Table 13. Continued.

(c) Run 3

SUMMARY FOR 9 RUNS/PHASES
TRANSFORMATION MATRIX IN TOTAL ITERATIONS

~~RUN 3~~

	TACH	ADF	WINDOW	MKR BCN	ALT	ART HOR	AIRSPD	IVSI	DR GYRO	TRN BNK	VOR 1	DME	VOR 2	
TACH	0	0	0	0	0	0	0	0	0	0	0	0	0	
ADF	0	10	0	0	1	1	0	0	0	0	0	0	0	
WINDOW	0	0	0	0	0	0	0	0	0	0	0	0	0	
MKR BCN	0	0	0	348	2	20	0	0	3	3	0	0	0	
ALT	0	1	0	1	970	56	0	4	7	2	0	0	1	
ART HOR	0	1	0	26	58	9517	12	1	96	93	0	0	0	
AIRSPD	0	0	0	1	1	13	209	1	0	5	0	0	0	
IVSI	0	0	0	0	1	5	0	50	2	0	0	0	0	
DR GYRO	0	0	0	1	8	95	0	2	1744	15	0	0	0	
TRN BNK	0	0	0	0	3	95	9	0	14	2114	0	0	1	
VOR 1	0	0	0	0	0	0	0	0	0	0	1	0	0	
DME	0	0	0	0	0	1	0	0	0	0	0	2	0	
VOR 2	0	0	0	0	0	0	0	0	0	2	0	0	8	
TOTAL	0	12	0	377	1044	9803	230	58	1866	2234	1	2	10	15637
OCCURRENCES	0	2	0	29	74	286	21	8	122	120	0	0	2	

Table 13. Continued.

(d) Run 4

SUMMARY FOR 9 RUNS/PHASES
TRANSFORMATION MATRIX IN TOTAL ITERATIONS

~~RUN 4~~

	TACH	ADF	WINDOW	MKR BCN	ALT	ART HOR	AIRSPD	IVSI	DR GYRO	TRN BNK	VOR 1	DME	VOR 2	
TACH	0	0	0	0	0	0	0	0	0	0	0	0	0	
ADF	0	18	0	0	3	0	0	0	0	0	0	0	0	
WINDOW	0	0	0	0	0	0	0	0	0	0	0	0	0	
MKR BCN	0	0	0	13	0	2	0	1	0	0	0	0	0	
ALT	0	1	0	2	2929	197	1	20	8	0	0	0	0	
ART HOR	0	2	0	1	183	22475	50	22	350	6	4	3	0	
AIRSPD	0	0	0	0	3	56	927	1	2	0	0	0	0	
IVSI	0	0	0	0	15	32	1	644	24	0	1	0	0	
DR GYRO	0	0	0	0	20	336	8	26	5784	4	0	3	0	
TRN BNK	0	0	0	0	2	3	2	0	3	192	0	0	1	
VOR 1	0	0	0	0	2	2	0	2	0	0	43	0	0	
DME	0	0	0	0	0	1	0	2	2	0	1	30	0	
VOR 2	0	0	0	0	0	0	0	0	0	1	0	0	7	
TOTAL	0	21	0	16	3157	23104	989	718	6173	203	49	36	8	34474
OCCURRENCES	0	3	0	3	228	629	62	74	389	11	6	6	1	

ORIGINAL PAGE IS OF POOR QUALITY

Table 13. Continued.

(e) Run 5

SUMMARY FOR 9 RUNS/PHASES
TRANSFORMATION MATRIX IN TOTAL ITERATIONS

~~RUN 5~~

	TACH	ADF	WINDOW	MKR BCN	ALT	ART HOR	AIRSPD	IVSI	DR GYRO	TRN BNK	VOR 1	DME	VOR 2	
TACH	0	0	0	0	0	0	0	0	0	0	0	0	0	
ADF	0	26	C	0	1	3	0	0	0	0	0	0	0	
WINDOW	0	0	0	0	0	0	0	0	0	0	0	0	0	
MKR BCN	0	0	0	6	0	C	0	1	0	0	0	0	0	
ALT	0	2	0	1	579	33	0	10	2	0	0	0	0	
ART HOR	0	3	0	0	33	9457	39	14	102	79	2	0	0	
AIRSPD	0	0	0	0	1	39	751	0	4	11	0	0	0	
IVSI	0	0	0	0	3	23	0	367	5	0	0	0	0	
DR GYRO	0	0	0	0	5	100	0	4	2030	24	2	0	0	
TRN PNK	0	0	0	0	3	73	16	0	21	1912	0	0	0	
VOR 1	0	0	0	0	0	2	0	1	1	0	37	0	0	
DME	0	0	0	0	0	0	0	0	0	0	0	0	0	
VCR 2	0	0	0	0	0	0	0	0	0	0	0	0	0	
TOTAL	0	31	0	7	625	9730	806	397	2165	2026	41	0	0	15828
OCCURRENCES	0	5	0	1	46	273	55	30	135	114	4	0	0	

Table 13. Continued.

(f) Run 6

SUMMARY FOR 9 RUNS/PHASES
TRANSFORMATION MATRIX IN TOTAL ITERATIONS

~~RUN 6~~

	TACH	ADF	WINDOW	MKR BCN	ALT	ART HOR	AIRSPD	IVSI	DR GYRO	TRN BNK	VOR 1	DME	VOR 2	
TACH	0	0	0	0	0	0	0	0	0	0	0	0	0	
ADF	0	13	0	0	0	2	0	0	0	0	0	0	0	
WINDOW	0	0	0	0	0	0	0	0	0	0	0	0	0	
MKR BCN	0	0	0	45	0	8	0	0	0	0	0	0	0	
ALT	0	1	0	3	3700	196	2	17	28	2	7	5	0	
ART HOR	0	1	0	4	220	30238	24	44	449	12	46	8	6	
AIRSPD	0	0	0	0	1	28	690	0	3	1	0	0	0	
IVSI	0	0	0	0	11	28	1	826	16	0	37	0	0	
DR GYRO	0	0	0	0	25	452	4	22	8687	12	59	7	2	
TRN BNK	0	0	0	0	0	12	3	0	13	351	0	0	3	
VOR 1	0	0	0	1	6	81	1	10	48	0	2238	3	0	
DME	0	0	0	0	2	10	0	1	14	0	2	172	0	
VOR 2	0	0	0	0	0	3	0	0	6	2	0	1	78	
TOTAL	0	15	0	53	3965	31058	725	920	9264	380	2389	196	89	49054
OCCURRENCES	0	2	0	8	265	820	35	94	577	29	151	24	11	

Table 13. Continued.

(g) Run 7

SUMMARY FOR 9 RUNS/PHASES
TRANSFORMATION MATRIX IN TOTAL ITERATIONS

~~RUN 7~~

	TACH	ADF	WINDOW	MKR BCN	ALT	ART HOR	AIRSPD	IVSI	DR GYRO	TRN BNK	VOR 1	DME	VOR 2	
TACH	0	0	0	0	0	0	0	0	0	0	0	0	0	
ADF	0	44	0	0	0	0	0	0	2	0	0	0	0	
WINDOW	0	0	11	0	0	0	0	0	0	0	0	0	0	
MKR BCN	0	0	0	133	1	14	0	0	0	0	0	0	0	
ALT	0	0	0	8	6237	392	2	31	32	1	3	0	5	
ART HOR	0	2	0	9	407	59821	84	61	842	181	105	7	139	
AIRSPD	0	0	0	0	1	82	1758	1	5	29	1	0	2	
IVSI	0	0	0	0	8	59	0	1552	38	0	30	0	5	
DR GYRO	0	0	0	0	44	901	2	21	19421	57	71	36	56	
TRN BNK	0	0	0	0	5	138	36	0	64	4383	2	1	29	
VOR 1	0	0	0	0	1	94	1	27	87	2	4746	6	11	
DME	0	0	0	0	0	4	0	0	41	0	14	740	5	
VOR 2	0	0	0	0	2	167	3	0	69	16	3	7	5727	
TOTAL	0	46	11	150	6706	61672	1886	1693	20601	4669	4975	797	5979	109185
OCCURRENCES	0	2	0	17	469	1851	128	141	1180	286	229	57	252	

Table 13. Concluded.

(h) Run 8

GENERAL AVIATION SIMULATION STUDIES OF PROBLEMS IN THE SINGLE PILOT IFR (SPIFR) FLIGHT ENVIRONMENT

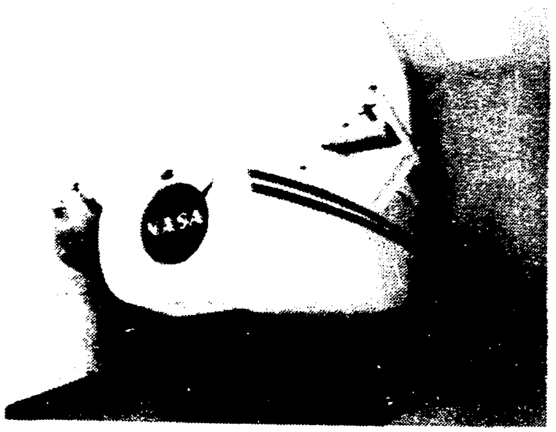

SIMULATOR CAPABILITY

- MOTION BASE
- CONTROL LOADER (YOKE)
- VLDS (VISUAL SCENE)
- SIDE WINDOW VIEW
- OCULOMETER
- ENGINE AND AIRSTREAM NOISE
- ATC STATIONS/COMMUNICATIONS
- ATLANTA OR NORFOLK/WASHINGTON AREA NAV AIDS
- AUTOPILOT
- VARIETY OF AIRPLANE TYPES

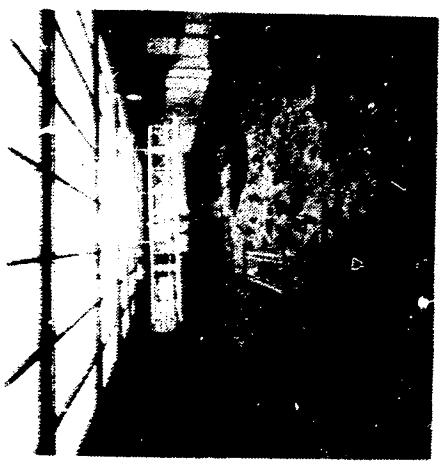

Figure 1.- Description of General Aviation Simulation.

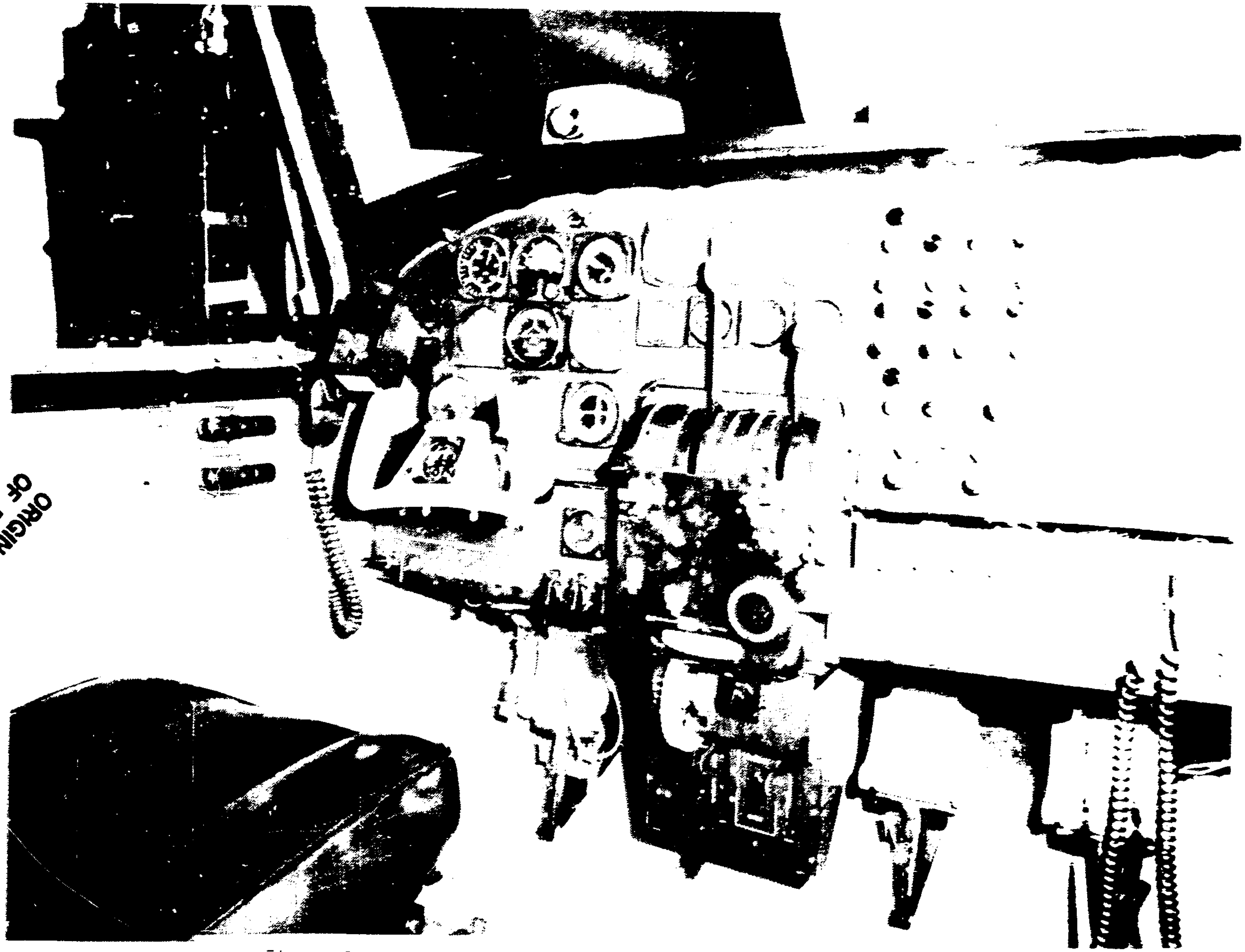

Figure 2.- Instrument panel in General Aviation simulator cockpit.

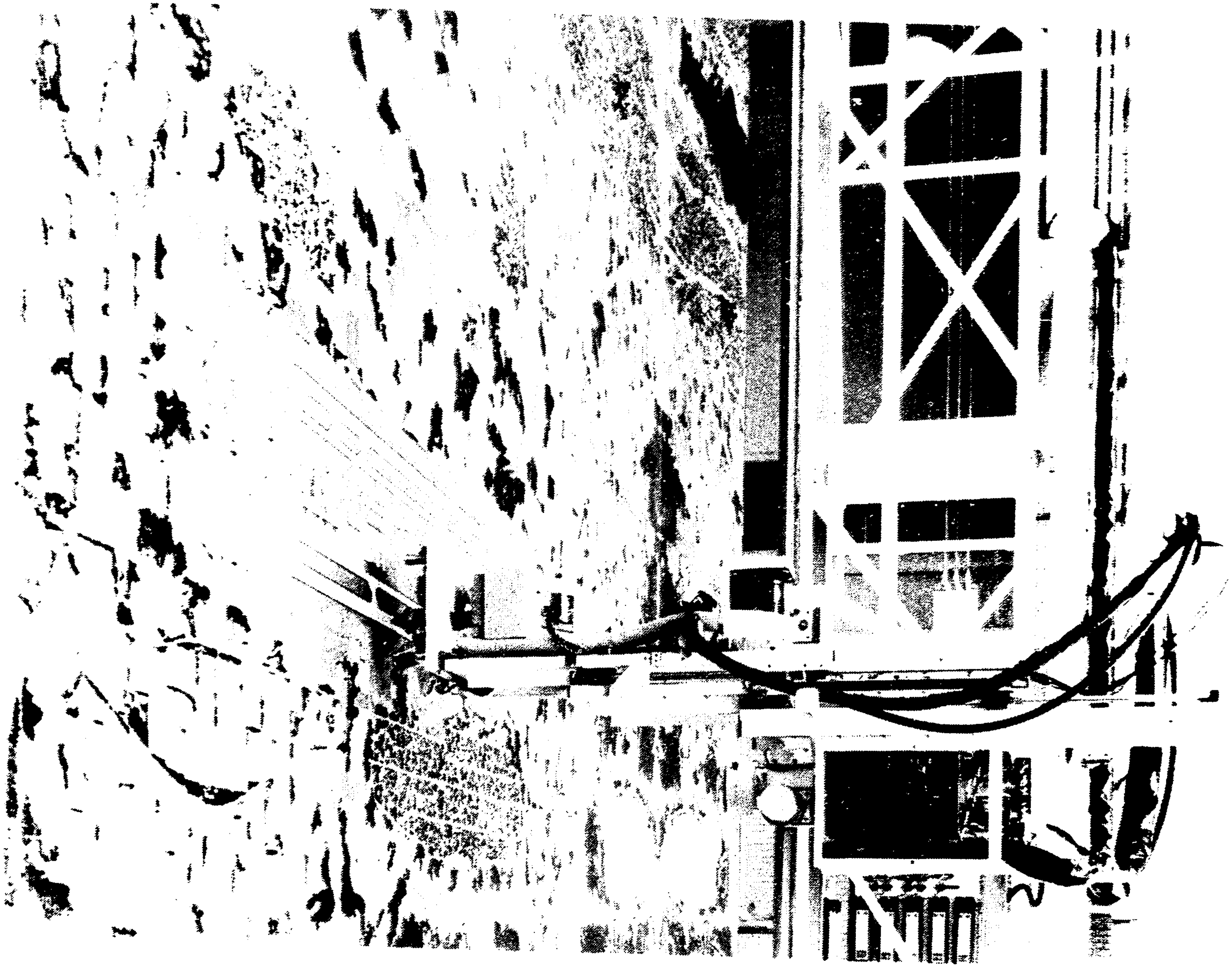

Figure 3.- Visual landing display system.

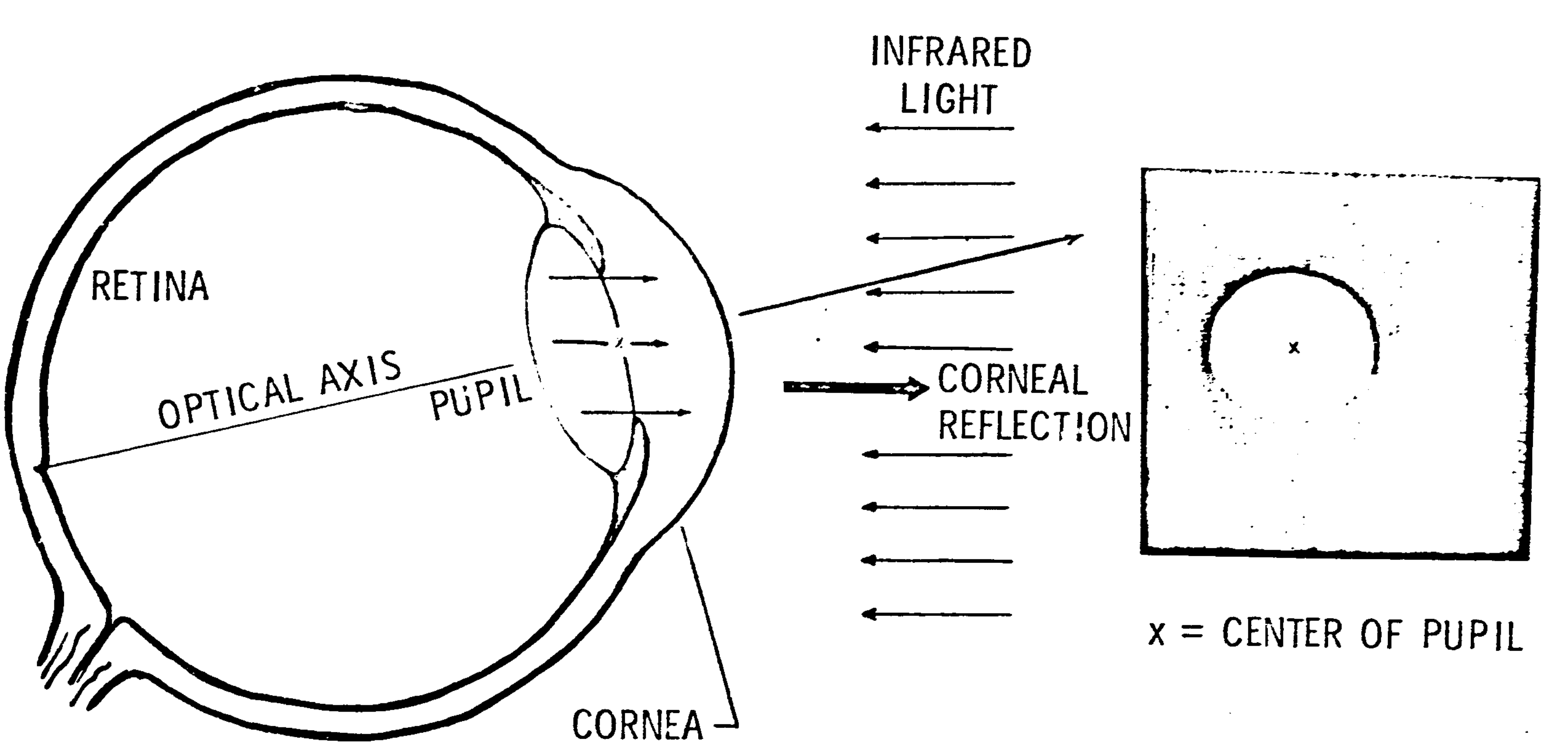

Figure 4.- Oculometer operating principle.

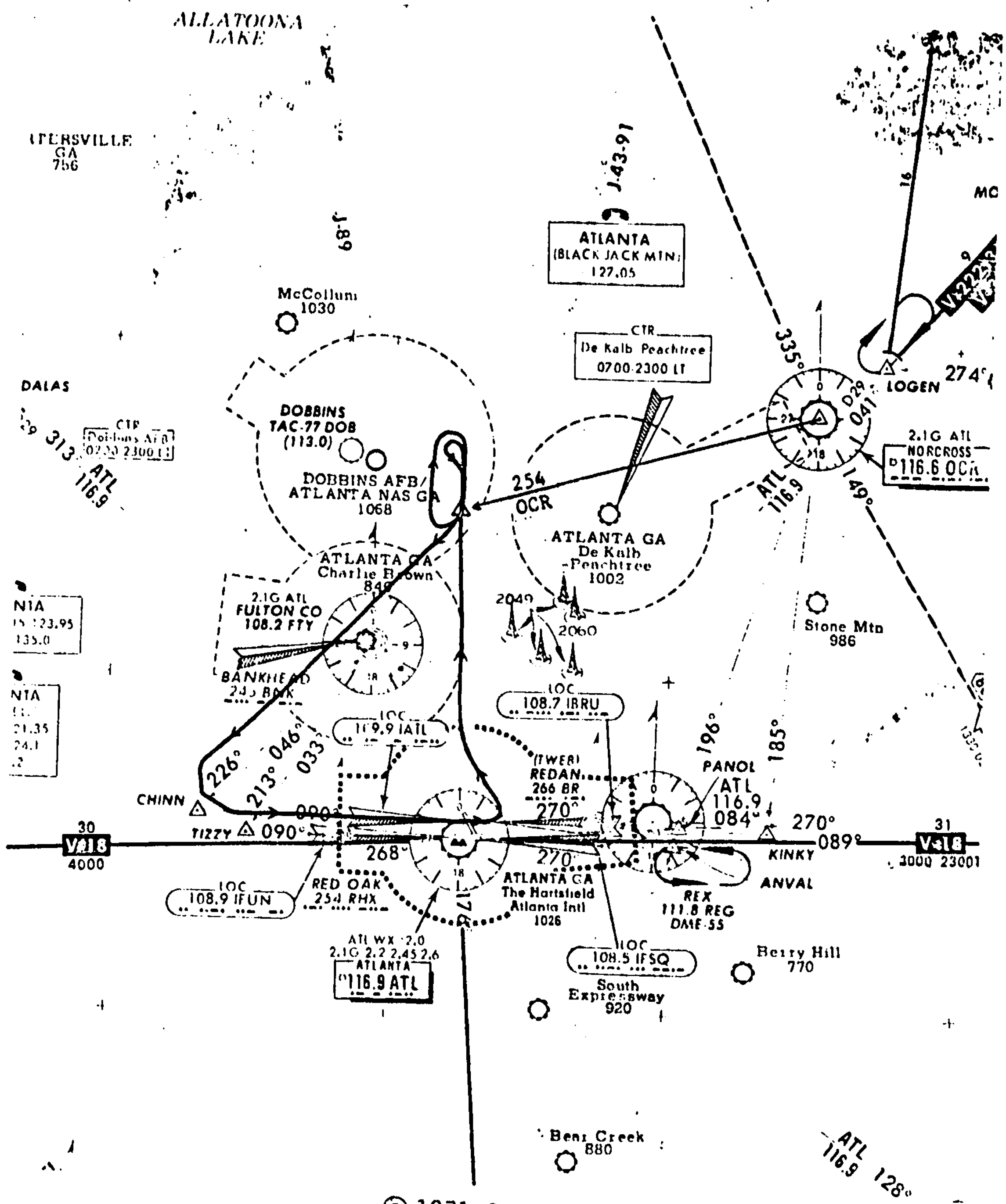

Figure 5.- Diagram of holding pattern flown in run 9. (not for navigational purposes; additions and deletions have been made to this chart).

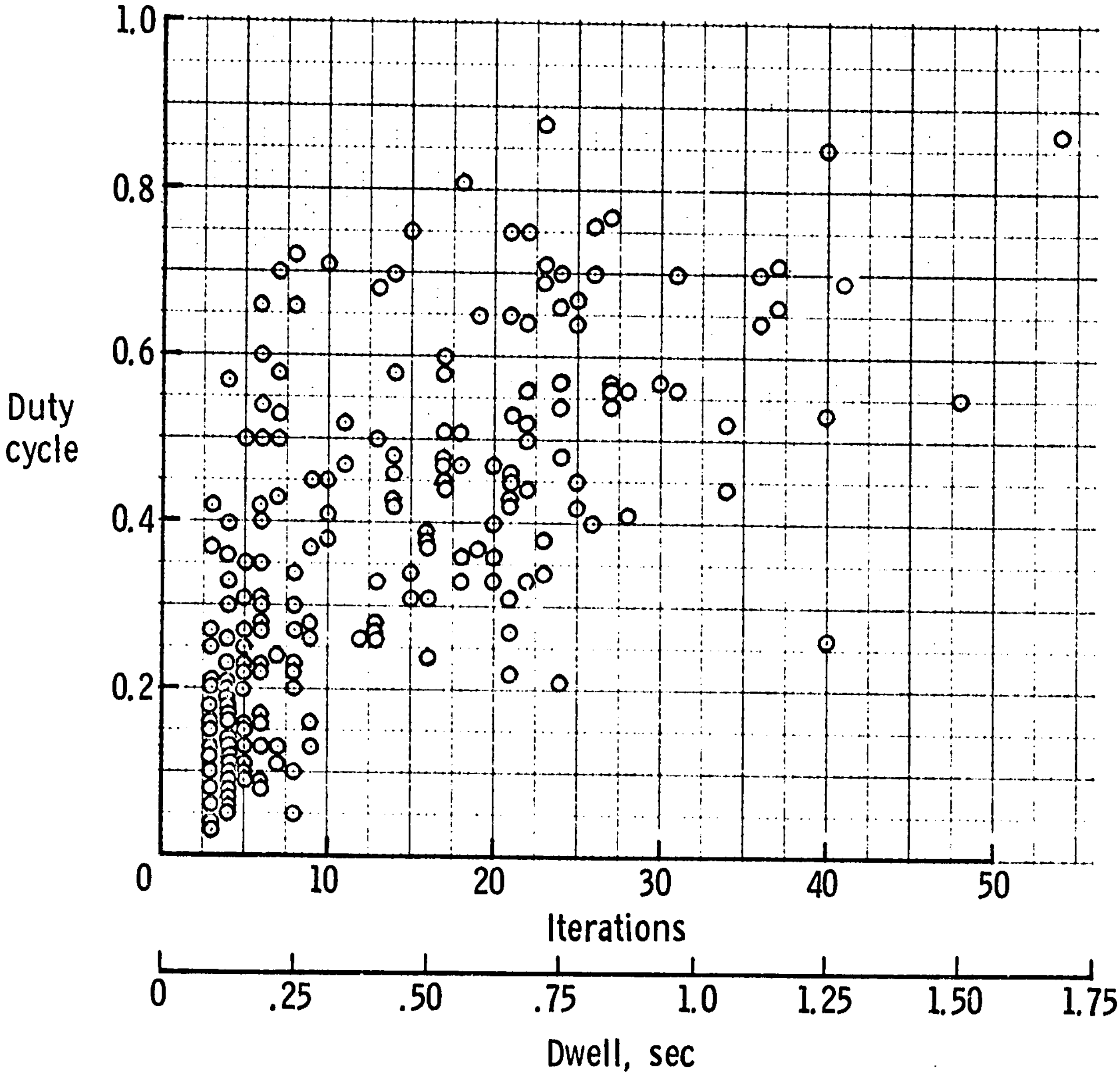

Figure 6. - Dwell and duty cycle of looks at directional gyro, Pilot C in phases 95-96.

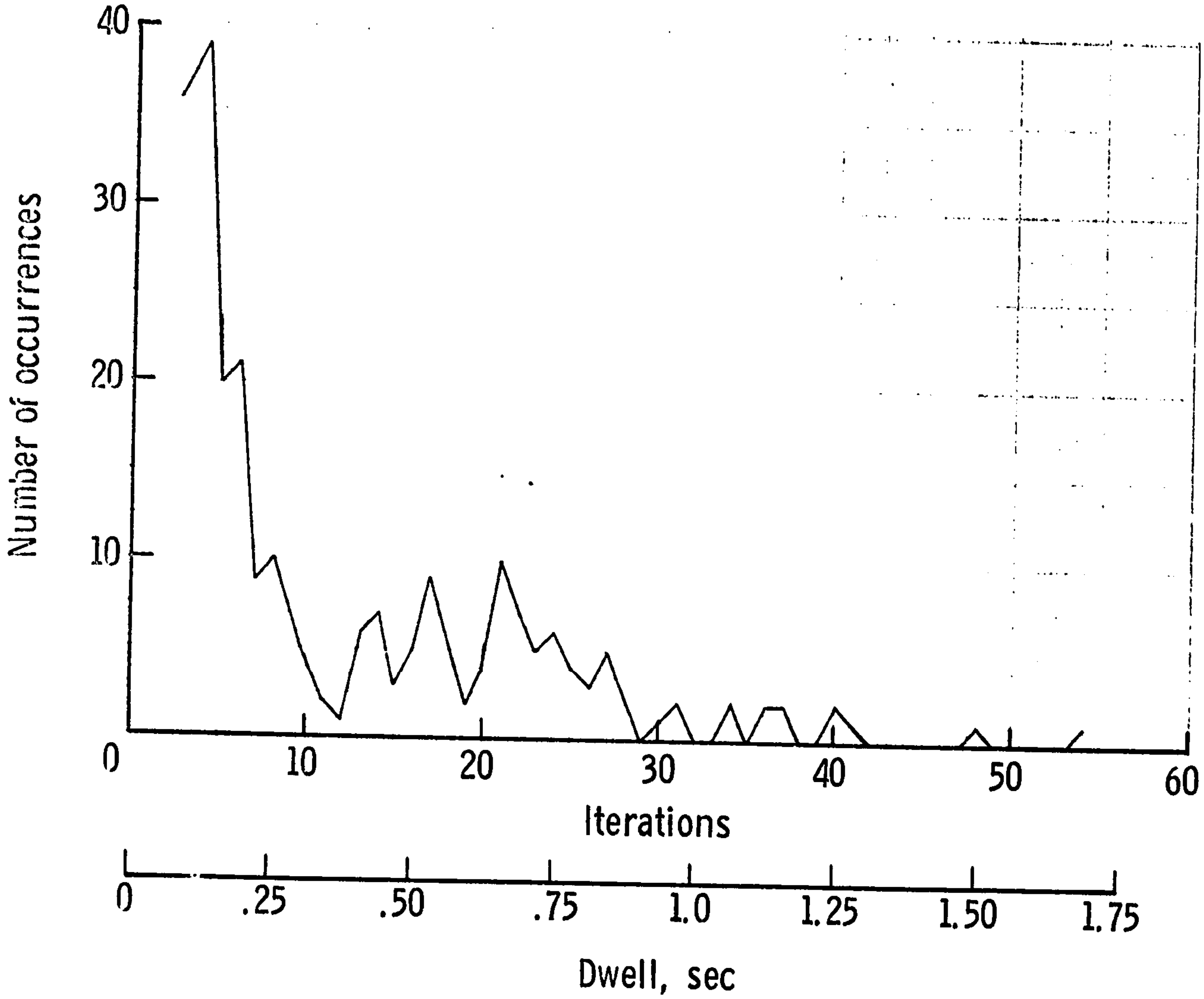

Figure 7. - Distribution of dwell times, Pilot C in phases 95-96.

ORIGINAL PAGE IS
OF POOR QUALITY

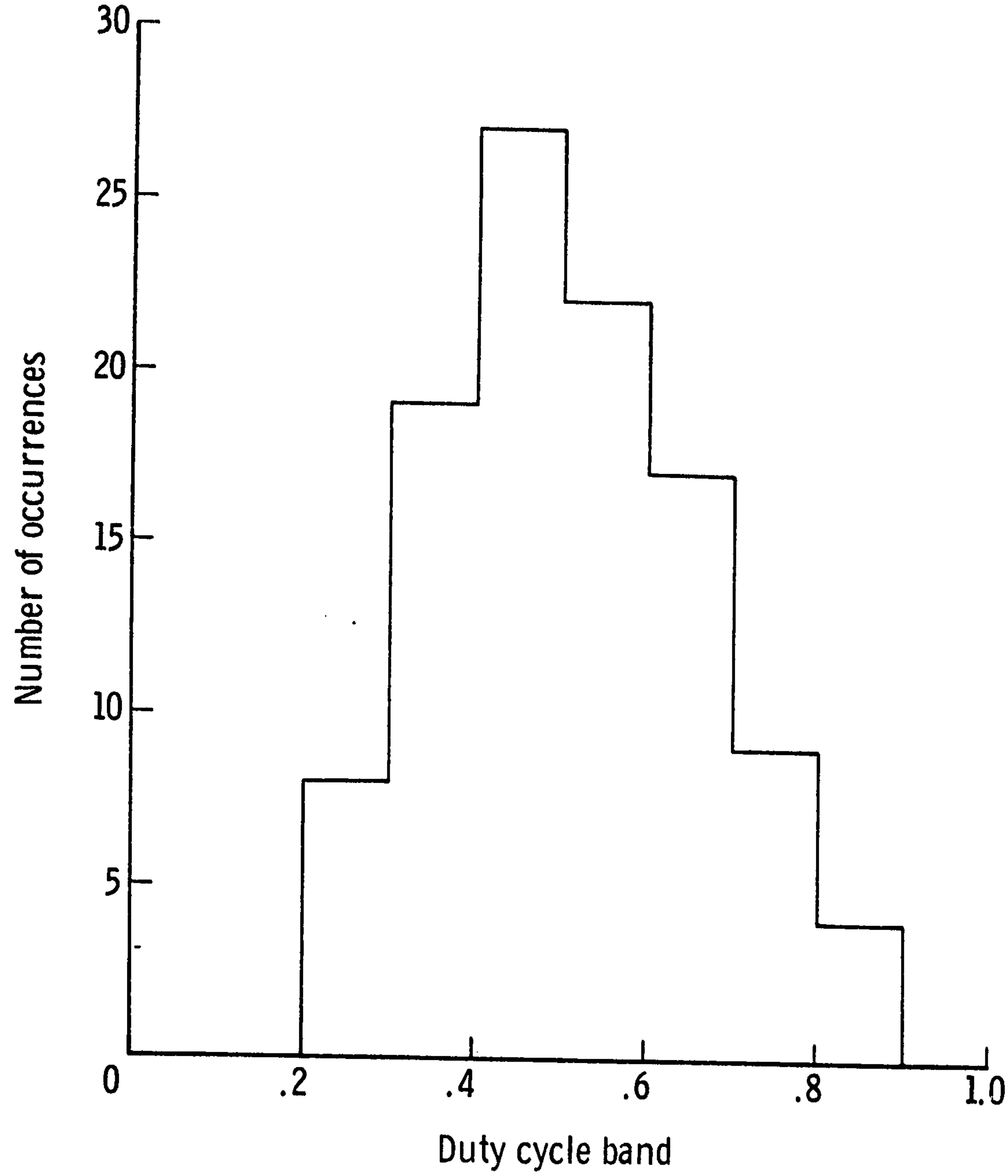

Figure 8. - Number of occurrences in duty cycle intervals, Pilot C in phases 95-96.

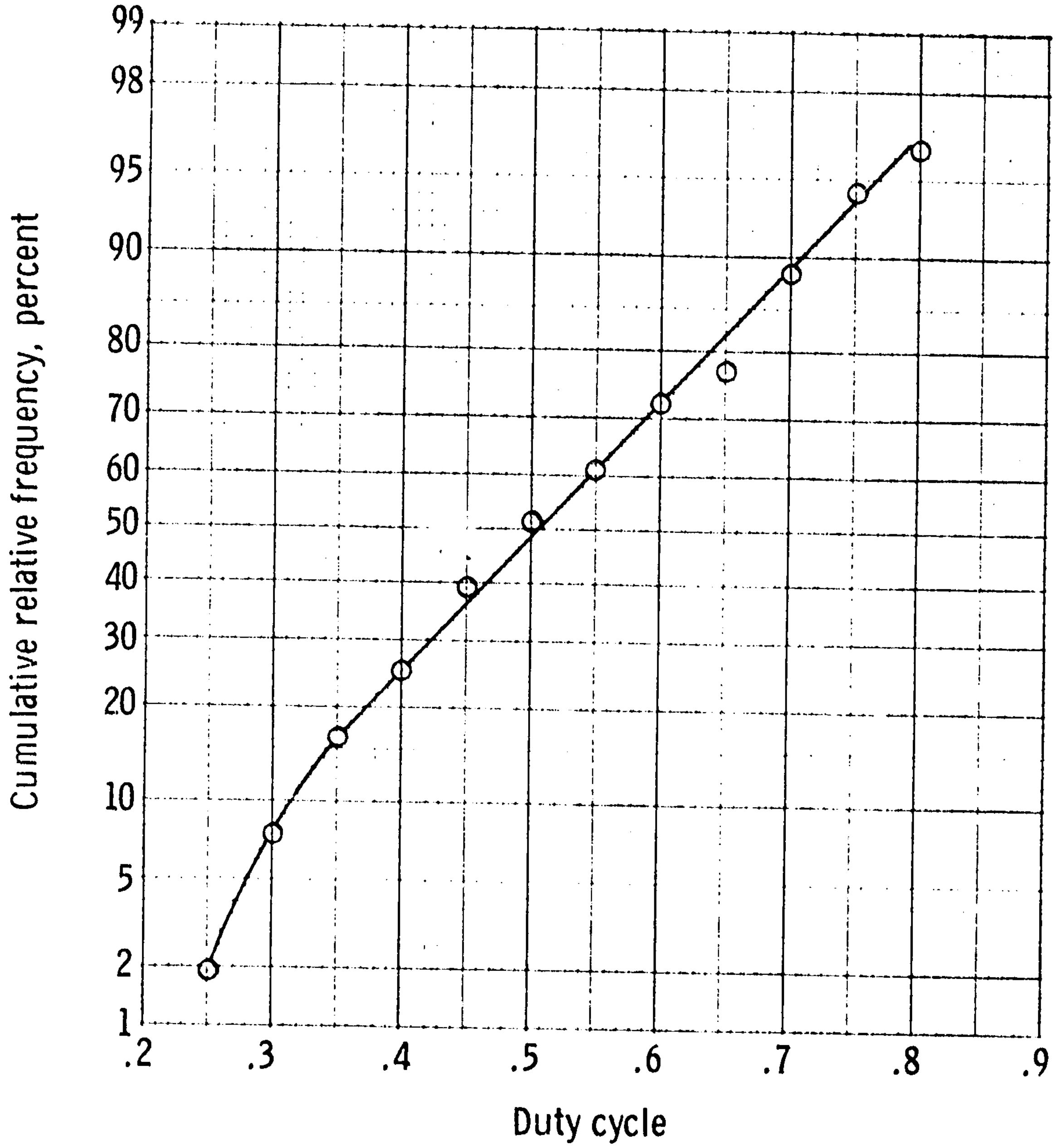

Figure 9. - Cumulative frequency distribution of duty cycle for directional gyro, Pilot C, phases 95-96.

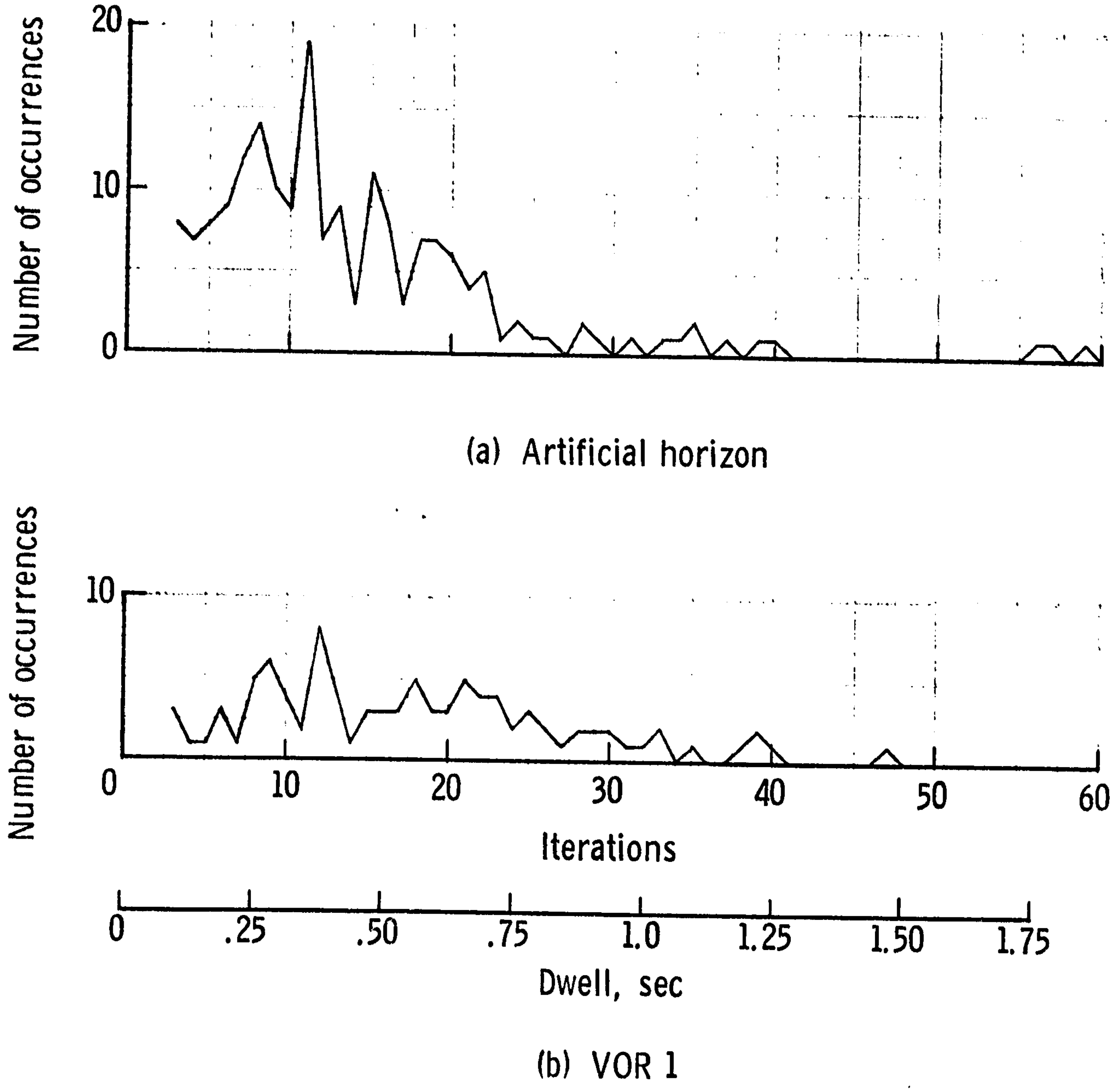

Figure 10.- Distribution of dwell times, Pilot C, phases 95-96.

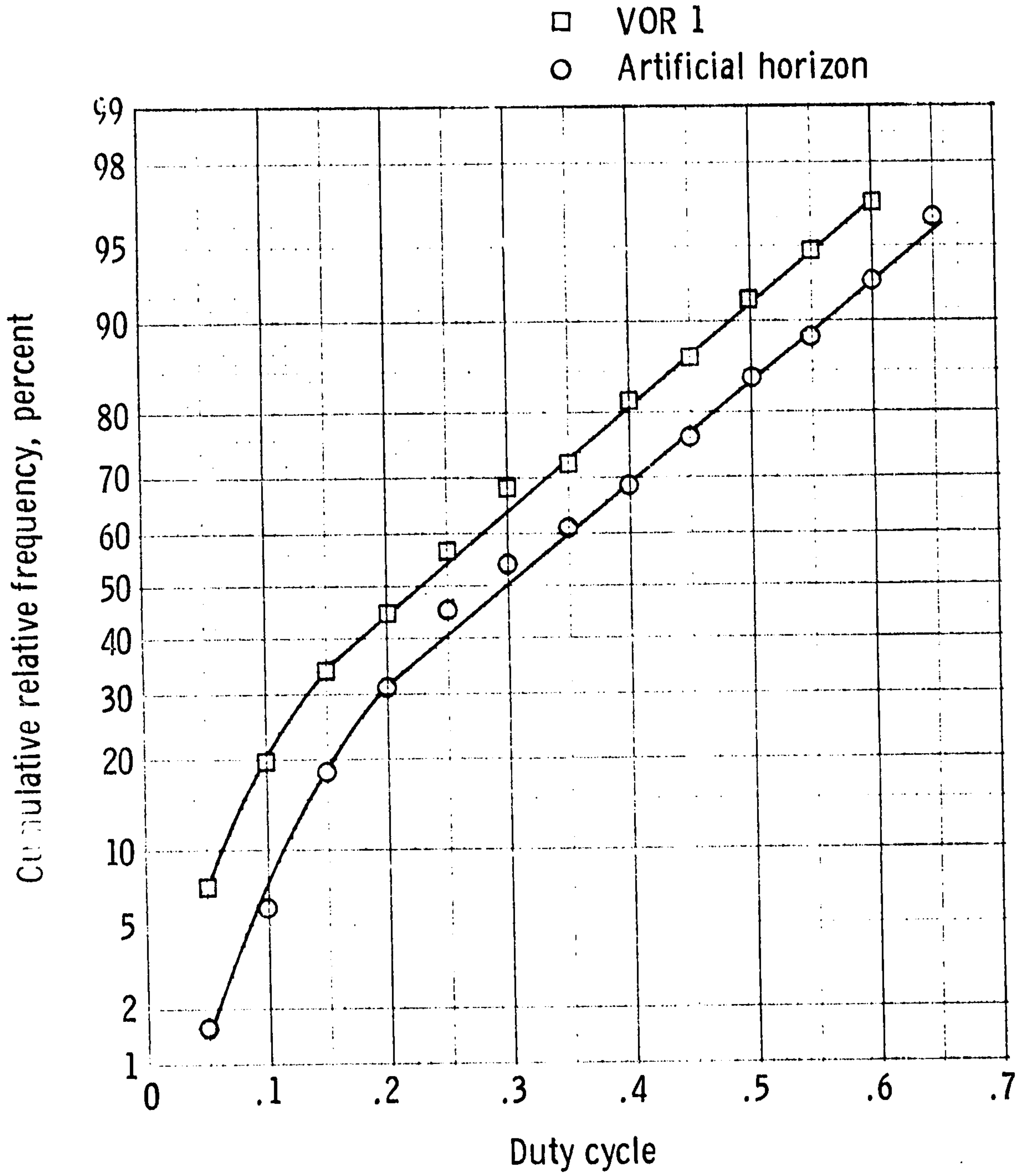

Figure 11. - Cumulative frequency distribution of duty cycle, Pilot C, phases 95-96.

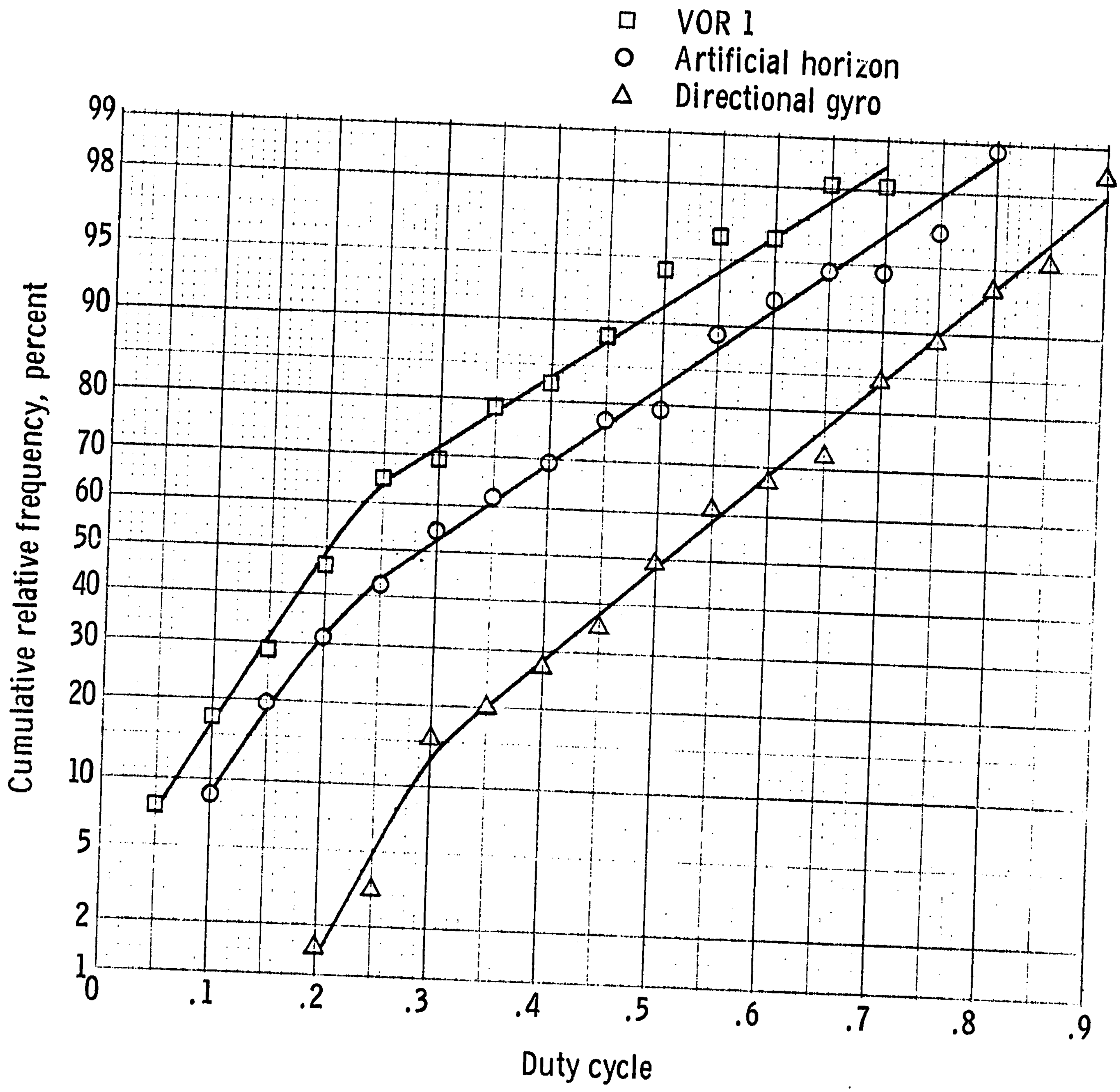

Figure 12. - Cumulative frequency distribution of duty cycle, Pilot C, phases 91-93.

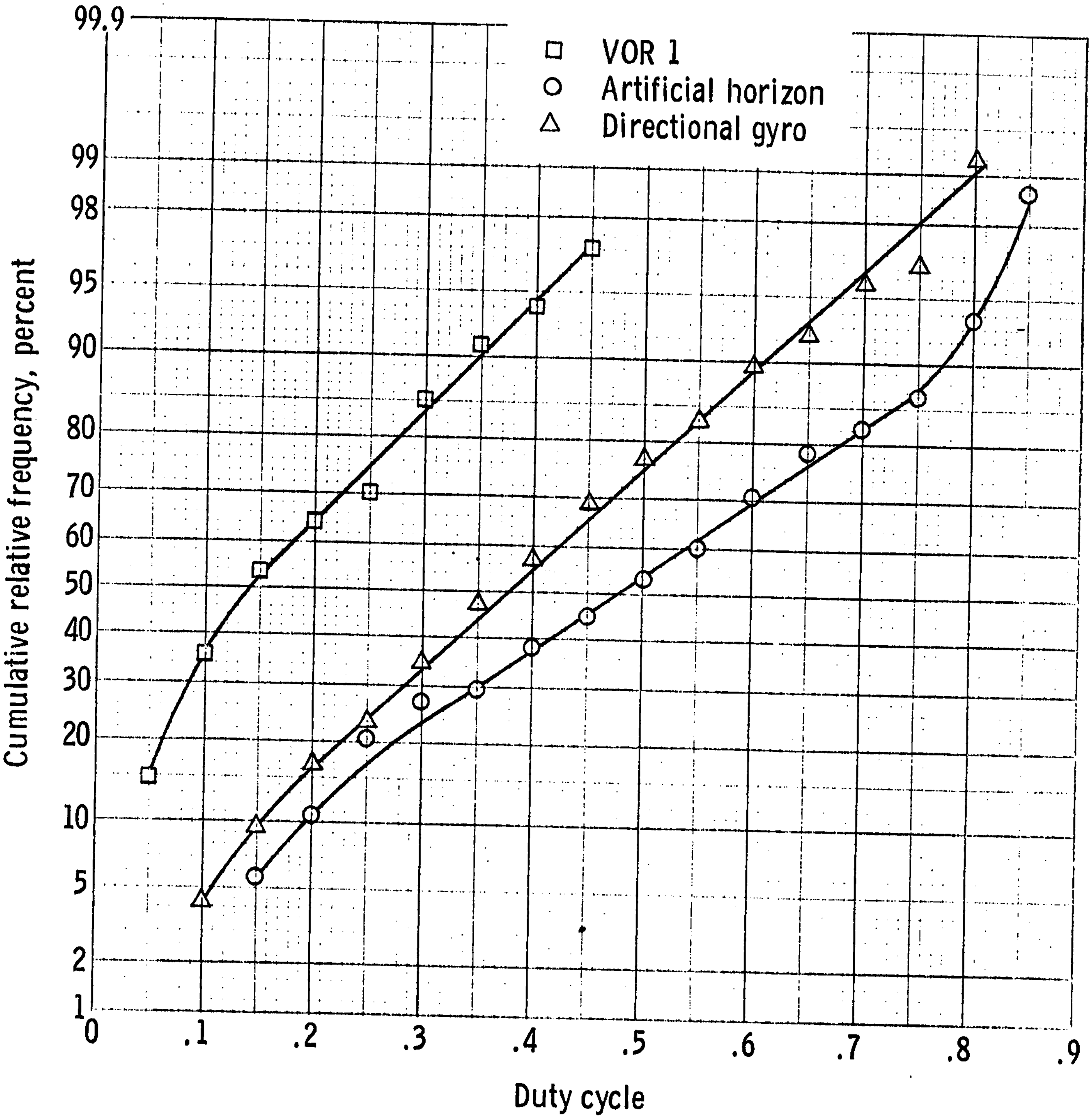

Figure 13. - Cumulative frequency distribution of duty cycle, Pilot A, phases 95-96.

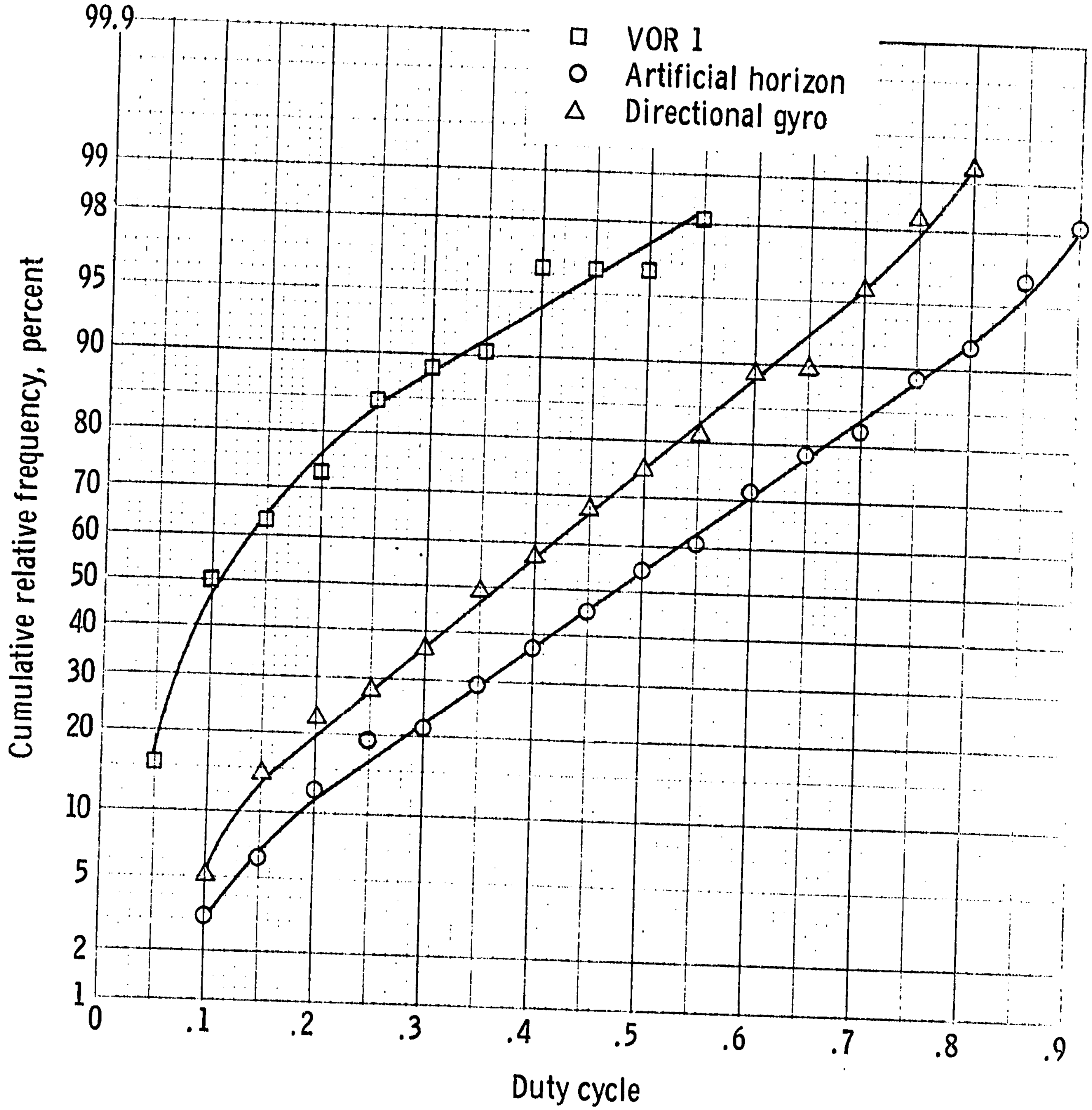

Figure 14. - Cumulative frequency distribution of duty cycle, Pilot A, phases 91-93.